Fluorescent cytoskeletal markers reveal associations between the actin and microtubule cytoskeleton in rice cells

Zengyu Liu[1], Isabella Østerlund[2,3], Felix Ruhnow[2], Yiran Cao[1], Guoqiang Huang[1], Wenguo Cai[1], Jiao Zhang[1], Wanqi Liang[1], Zoran Nikoloski[3], Staffan Persson[1,2,4]*, Dabing Zhang[1,5]*

[1] Joint International Research Laboratory of Metabolic and Developmental Sciences, School of Life Sciences and Biotechnology, Shanghai Jiao Tong University, Minhang 200240, Shanghai, China;

[2] Department of Plant & Environmental Sciences (PLEN), University of Copenhagen, 1870 Frederiksberg, Denmark

[3] Systems biology and Mathematical Modelling, Max Planck Institute of Molecular Plant Physiology, Am Mühlenberg 1, 14476 Potsdam-Golm, Germany

[4] Copenhagen Plant Science Center (CPSC), University of Copenhagen, 1870 Frederiksberg, Denmark

[5] School of Agriculture, Food, and Wine, University of Adelaide, Waite Campus, Urrbrae, South Australia 5064, Australia

* Corresponding authors: zhangdb@sjtu.edu.cn (D.Z.) and staffan.persson@plen.ku.dk (S.P.)

Key words: Cytoskeleton, actin, microtubule, fluorescent markers, live cell imaging, rice

Summary statement:

We generated rice cytoskeleton fluorescent marker lines and investigated cytoskeletal organization and associations in living rice cells. We exemplify the utility of the marker lines in a range of tissues and biological processes, delivering new and exciting results on rice cell biology and cytoskeleton associations.

Abstract

Rice (*Oryza sativa*) is one of our main food crops, feeding around 3.5 billion people worldwide. An increasing number of studies note the importance of the cytoskeleton, including actin filaments and microtubules, on rice development and environmental responses. Yet, reliable *in vivo* cytoskeleton markers are lacking in rice, which critically limits our knowledge of cytoskeletal functions in living cells. Therefore, we generated bright fluorescent marker lines of the actin and microtubule cytoskeletons in rice, suitable for live cell imaging in a wide variety of rice tissues. Using these lines, we show that actin bundles and microtubules engage and co-function during pollen grain development, how the cytoskeletal components are coordinated during root cell development and that the actin cytoskeleton is robust and facilitates microtubule responses during salt stress. Hence, we conclude that our cytoskeletal marker lines, highlighted by our exciting findings of cytoskeletal associations and dynamics, will substantially further future investigations in rice biology.

Introduction

Rice (*Oryza sativa*) is one of the staple food crops for billions of people around the world (Seck et al., 2012). Understanding response mechanisms of rice to diverse intra- and extra- cellular signals is tightly linked to improvements of rice performance. The plant cytoskeleton, composed of filamentous actin and microtubules, critically support plant development and stress resistance in plants (Kost et al., 1999; Wang and Mao, 2019), including rice. While most of the plant cytoskeleton studies have been made in the model dicot plant *Arabidopsis thaliana*, there are also a few studies that highlight the importance of the cytoskeleton in rice development and environmental responses. For example, both actin- and microtubule-related rice mutants displayed severe developmental defects (Komorisono et al., 2005; Zhang et al., 2010), microtubule-related proteins were frequently reported to control rice seed size (Sun et al., 2017; Yang et al., 2020) and several rice cytoskeleton proteins were found to impact stress resistance (Xu et al., 2018; Lo et al., 2020). Therefore, it is important to study the cytoskeleton in detail in rice.

Most of the rice cytoskeleton reports focus on mutant characterization, with negligible *in vivo* cytoskeleton investigations (Zhang et al., 2010; Li et al., 2014; Huang et al., 2018; Song et al., 2019; Lo et al., 2020; Chang et al., 2021). In particular, important processes in rice, including tillering, underwater growth, pollen development, and seed quality, have not yet been studied in connection with cytoskeleton despite its prominent roles in these processes. Whereas static studies by immuno-labelling are dominating the rice cytoskeleton field, live cell imaging is superior since the cytoskeleton is composed of highly dynamic structures (Shaw et al., 2003; Sheahan et al., 2004). To this end, bright and stable fluorescent markers of the cytoskeletons are much needed. However, fluorescent cytoskeleton marker lines have only been established in some plant species, e.g. Arabidopsis, Medicago (*Medicago truncatula*), maize (*Zea mays*) and cotton (*Gossypium spp*) (Shaw et al., 2003; Antonius et al., 2007; Mohanty et al., 2009; Yu et al., 2019). These studies have highlighted the importance of selecting suitable fluorescent tags and cytoskeleton labelling proteins to, i) minimize their influence on cytoskeletal behaviour, and ii) allow long-term visualization of the cytoskeletal structures (Sheahan et al., 2004). The fine-actin binding domain 2 of Arabidopsis fimbrin 1 (fABD2), mTalin and lifeact are commonly used for actin labelling (Kost et al., 1998; Sheahan et al., 2004; Qu et al., 2017), while tubulin subunits and the mammalian microtubule binding protein 4 (MAP4) are typical proteins for microtubule labelling (Marc et al., 1998; Ueda et al., 1999; Shaw et al., 2003). Notably, these labelling proteins may impact the behaviour of the cytoskeletons and so the protein abundance and biochemical properties of marker proteins are important factors to consider (Courtemanche et al., 2016). However, the impact of the marker proteins appear to differ among different organisms. That may be the reason why one construct performs well in one specie or tissue, but not in another (Vidali et al., 2009; Flores et al., 2019), emphasizing the need to choose suitable components to construct markers for specific plants or tissues.

In this study, we generated effective rice fluorescent cytoskeleton marker lines, including that of filamentous actin and microtubules, allowing live cell imaging of the rice cytoskeleton. With our marker lines, we explored several cytoskeleton-related topics in rice biology, including actin and microtubule interplay during pollen development and root cell division, salt response and cytoskeletal mutant characterization. We thus describe several exciting phenomena, which will open up for further investigations on rice cytoskeleton functions.

Results

Generation of cytoskeleton markers in rice

To study cytoskeletal dynamics in rice *in vivo*, we set out to generate fluorescent marker lines for the microtubule and actin cytoskeleton. We generated a range of different combinations of promoters, fluorescent proteins and cytoskeleton-labelling proteins (Fig. 1). We transformed these into wild-type rice plants and screened multiple independent transgenic lines in T2 generation. The advantages and disadvantages of these tested components are compared and summarized in Table S1. We found that the monocot ubiquitin promoters including rice ubiquitin 2 (*RUBQ*) and maize ubiquitin 1 (*Ubi1*) gave homogenous fluorescent signals in rice cells, while the tobacco virus promoter 35S often was silenced (Fig. 1A, B). *RUBQ* lines typically showed brighter signals than *Ubi1* driven lines. Inspired by Arabidopsis studies, we tried the domain of mouse Microtubule Association Protein 4 (MAP4) and the rice Tubulin subunit Alpha 1 (OsTUA1) to label rice microtubules, and Arabidopsis actin binding protein fABD and its rice homolog OsfABD to label rice actin filaments, respectively. In the resulting transgenic lines, OsTUA1 labelled rice microtubules weakly but substantial fluorescence was also observed of the cytosol (see the white arrow heads in Fig. 1B). No signal was detected in the OsfABD lines (the second panel of Fig. 1A). Fortunately, MAP4 and fABD lines effectively labelled the microtubule and actin cytoskeleton in rice plants (right three panels in Fig. 1A, B). Notably, fABD lines were developmentally indistinguishable from wild type plants,

whereas the MAP4 lines occasionally caused some growth defects also reported for different microtubule marker lines in Arabidopsis (Fig.S1A). However, wild-type like MAP4 transgenic lines were also frequently obtained (Fig.S1B). Among the fluorescent proteins we used, the bright green fluorescent protein mNeongreen (mNG) appeared bright and stable, while the red fluorescent protein mScarlet was bright but prone to photo-bleaching (Fig. S1C, D).

We first visualized the cytoskeleton throughout different rice tissues, including roots, root hairs, stem, leaves, stomata, anthers, pollen grains and pollen tubes (Fig. 2A , B). Bright fluorescence was observed in all tissues, except in the pollen mother cell before microspore formation (Fig. S2). Overall, we observed brighter fluorescence in younger plant tissues. To sum up, our marker lines can be used to image the organization and dynamic behavior of the cytoskeleton in both vegetative and reproductive tissues (Fig. 2C, D, movie S1, S2), including cells with different growth modes.

Live cell imaging reveals dramatic reorganization of the cytoskeleton during rice pollen development

Using our marker lines, we set out to explore a range of processes related to the cytoskeletons. We first imaged cytoskeletal behaviour during rice pollen development. As shown in Fig. 3, both the actin and microtubule cytoskeletons are fragmented in young microspores (left panel). Short actin filaments and microtubules subsequently formed during pollen grain development (bright field panels from left to right in Fig. 3). Both actin filaments and microtubules gradually extend as the pollen grains increased in size; however, the polymers lacked clear common directionality. During pollen grain maturation and amyloplast formation (the red asterisks in Fig. 3), both the actin and microtubule cytoskeletons form radial patterns radiating from the germination pore (indicated by yellow arrows in Fig. 3). Once the pollen is hydrated, the cytoskeleton gradually becomes disordered again, and partially depolymerized (right panels of Fig. 3).

The radial alignment of the actin and microtubule cytoskeletons prompted us to consider whether the two structures may perhaps function together and associate with each other. Therefore, we obtained actin and microtubule cytoskeleton dual-labelled lines (*RUBQ::mNG-fABD* and *RUBQ::mScarlet-MAP4*) by crossing the single marker lines. In the resulting lines, we observed bright fluorescence from both markers and subsequently observed actin and microtubule cytoskeletons simultaneously in mature pollen grains. Strikingly, we found that the two fluorescent signals overlapped (Fig. 4A, C). Indeed, the two markers showed 70% colocalization based on Pearson coefficient analyses (Fig. 4C). Closer observations revealed that thick actin bundles radiated out from the germination pores (indicated by the white arrowheads in Fig. 4D), whereas filamentous actin interspersed these bundles (indicated by the yellow arrowheads in Fig. 4D). Interestingly, the colocalization of actin and microtubule cytoskeleton occurred along the actin bundles, and not the fine filaments (as shown in Fig. 4D and Movie S3). This is consistent with colocalization analyses using Manders' coefficient test, in which up to 90% of the microtubule-related fluorescence colocalized with the fluorescence from the actin cytoskeleton, while only about 50% of the actin-related fluorescence colocalized with the microtubule signal (Fig. 4C).

To address if the two cytoskeletal structures are associated with each other in mature pollen grains, we recorded time-lapse imaging of the dual-labelled line. Here, we found that the microtubules were coordinated with the actin bundles (Fig. 4E, F), indicating a tight interplay between the two cytoskeletal structures. This indicated that there may be a mutual structural and perhaps a functional relationship between the cytoskeletal components in pollen grains. We investigated this by disrupting one of the polymers and observed if this resulted in any changes in the other one. When the actin cytoskeleton was partially depolymerized by actin inhibitor Latrunculin B, the number of microtubule polymers did not obviously change (Fig. 4G, Movie S4). However, the microtubule radial organization was perturbed and the engagement with actin decreased, i.e. the Pearson correlation coefficient between the microtubules and the remaining actin filaments was reduced (Fig. 4G and S3).

Notably, when the microtubules were depolymerized using Oryzalin, the radial actin bundles rapidly disappeared and were replaced with a myriad of cytosolic actin filaments (Fig. 4H, Movie S5). Overall, the Oryzalin treatment was accompanied with a reduction in actin filamentous fluorescence (middle panel in Fig. 4H). These observations indicate that the actin and microtubule cytoskeleton provide mutual structural support to each other during pollen grain development.

Actin and microtubule array reorganization in root cells of rice

Motivated by the cytoskeletal interactions in rice pollen, we next examined their relationship in other cell types, such as root cells. Here, microtubules play an essential role during cell division, and display distinct configurations at different division stages, including preprophase band, spindle and phragmoplast (Lipka et al., 2015). These configurations were also clearly observed in dividing rice root cells by our marker lines (Fig. 5). Actin filaments function in cell division (Maeda et al., 2020); however, the actin configurations during cell division remain controversial (Panteris, 2008). In rice root cells, the abundant actin filaments in non-dividing cells gradually disappeared during preprophase band formation (Fig. 5). At telophase, we detected scant actin cytoskeletal fluorescence (Fig. 5). However, we noted clear actin-related fluorescence during phragmoplast progression (indicated by arrow in Fig. 5); where the fluorescence appeared to be associated with the emerging cell plate. This observation is consistent with the reported cell plate-promoting function of actin cytoskeleton (Maeda and Higaki, 2021). Hence, by contrast to the pollen grains, the actin and microtubule cytoskeletons appear to function separately in dividing rice root cells. The disappearance of the actin cytoskeleton may coincide with reduced cytoplasmic streaming, which decrease during the onset of division in *Paramecium bursaria* (Sikora et al., 1991).

In interphase rice root cells, we did not detect any obvious association between the actin and microtubule cytoskeletons (Fig. 6A). As reported in Arabidopsis, transverse microtubule arrays in elongating root cells re-arrange towards a longitudinal direction during cell maturation and growth cessation (Chan, 2012; Adamowski et al., 2019).

We noted a similar reorientation also in developing rice roots (upper panel in Fig. 6A). Interestingly, we found a similar re-organization also of the actin cytoskeleton (lower panel in Fig. 6A). To quantify such change, we extracted filament edge angles using the Cytoseg2.0 algorithm (Nowak et al., 2020), and plotted the angles as circular histograms (Fig. 6B). We analyzed the perpendicularity (i.e. deviations from the cell growth axis of the filaments) and randomness (i.e. the degree of coherence of the filaments) of the resulting histograms (Fig. 6C, D). In agreement with our observations, both the actin and microtubule cytoskeletal arrays re-organized to align with the growth axis of the maturing cells (Fig. 6C). Whereas the actin array became increasingly more directional in maturing root cells, the microtubule array re-oriented in a coordinated fashion where the array maintained high directionality during the re-arrangement (Fig. 6C, D). We noted similar actin array re-organization also in other maturing cell types, such as anther epidermis (Fig. S4). We speculate that the cytoskeletal array re-organization may be a common procedure during interphase cell maturation.

The actin cytoskeleton sustains microtubule re-emergence during salt stress in rice root cells

Apart from supporting plant development, the cytoskeleton also plays crucial roles in adapting to changes in environmental conditions. For example, the microtubule array is sensitive to salt (NaCl) treatment, which causes rapid depolymerization in Arabidopsis (Endler et al., 2015). To assess how salt impacts the cytoskeletons in rice, dual-labelled rice seedlings (five days after the crown root emerged) were incubated in NaCl-containing (250 mM) liquid medium. As in Arabidopsis, microtubules rapidly de-polymerized and re-emerged over time (Fig. 7A; Table S2). The response period and extent correlated to seedling age and root cell type. The younger the seedling, the more rapidly it responded (Fig. S5). Microtubule adjustments, both de-polymerization and recovery, started from the root tip and progressively responded upwards along the root (Fig. S6). During microtubule de-polymerization, we observed apparent fluorescent foci. These were initially few and

relatively small, but gradually grew larger with time until microtubules disappeared (Fig. 7A from 2 h to 4 h; Table 1). During microtubule recovery, the large foci seemed to form new microtubules and we only observed small foci that gradually disappeared (Fig. 7A from 6 h to 8 h; Table 1). At later time points, microtubule arrays recovered and almost no foci were observed (Fig. 7A 8 h; Table 1, S2). However, the microtubule density never reached the levels of those prior to treatment (Fig. 7A, control vs 8 h; Table S2), 77.1 microtubule filaments per cell (counted from 10 control cells) compared with 13.79 in cells treated by salt for 8 h,, indicating that microtubule recovery was only partial. By contrast to the microtubule array, no major depolymerization events were observed for the actin cytoskeleton during the salt treatment. Indeed, actin filaments were abundant and maintained to a similar degree as those of the control cells (see the mNG-fABD channel in Fig. 7A). Therefore, we conclude that the actin cytoskeleton is more tolerant to salt stress than microtubules.

These results prompted us to investigate whether the actin cytoskeleton has a function in sustaining the microtubule response during salt stress. To assess this further, we looked at both actin cytoskeleton and microtubule dynamics during salt treatment. During microtubule disassembly, small microtubule-related fluorescent foci formed and subsequently began to merge to form larger foci (Fig. 7B). Interestingly, these events coincided with actin filaments (Fig. 7B; Movie S6). Moreover, simultaneous treatment with NaCl and the actin disruptor Latrunculin B delayed the formation of larger microtubule-related foci (Fig. 7C). Furthermore, separating microtubule-related foci associated with, and tracked along, actin filaments (Fig. 7D; Movie S7). Again, the disruption of the actin filaments caused a substantial delay in microtubule recovery (Fig. 7E). We therefore propose that actin filaments facilitate for rapid re-emergence of microtubules during salt exposure.

RMD supports actin bundling in rice coleoptile cells

Rice morphology determinant (RMD) encodes the rice formin 5 protein, which binds to and bundles actin filaments (Zhang et al., 2011). RMD controls many aspects of rice biological processes, including light responses (Fig. 8A and (Song et al., 2019)).

These results make *rmd* an ideal genotype to assess the actin array organization and behaviour using our actin fluorescent markers. We therefore crossed the *rmd-1* mutant lines with the *mNG-fABD* expressing line. We next investigated the actin array in both five-day-old dark and light-grown *rmd-1* coleoptile. We found that the actin cytoskeletal organization was different in the *rmd-1* as compared to that in wild type (Fig. 8B). Detailed inspection of the actin organization revealed less actin bundling in the *rmd-1* as compared to wild type. To quantify any differences in the actin array organization, we again employed Cytoseg2.0 (Nowak et al., 2020). Using this algorithm, we confirmed the reduced actin bundling in the *rmd-1* mutant (Fig. 8C). In addition, quantitative analyses revealed that the actin filaments were less coherent in the *rmd-1* as compared to wild type (Fig. 8D), and consequently aligned less well with the major cell axis (Fig. 8E). Interestingly, the actin bundling was significantly reduced in light-grown seedlings compared to dark-grown (Fig. 8B, C and Table S3), perhaps reflecting a role of actin bundles in rapid cell expansion. Interestingly, this scenario is reversed in the *rmd-1* mutant (Fig. 8B, C and Table S3). We also observed the microtubule array in *rmd-1*. Compared with wild type, the *rmd-1* displayed some disturbance in the microtubule array, notably in light-germinated coleoptiles (Fig. S7). However, the differences were less pronounced than those observed for the actin cytoskeleton. These differences may perhaps explain why the *rmd-1* mutant displays a shoot bending phenotype in light (Fig. 8A).

Discussion

We established bright and stable fluorescent cytoskeleton markers in rice to facilitate live cell imaging of the actin and microtubule cytoskeletons (Fig. 1, 2). We found that both *Ubi1* and *RUBQ2* promoters may be used to drive fABD and MAP4 to get homogeneous, bright, and stable actin and microtubule fluorescence. For microtubule labelling, we advise to use the *Ubi1* promoter since the high expression of the *RUBQ2* promoter tend to cause abnormal plant phenotypes (Fig. S1). Although the 35S promoter appears to induce silencing in many rice tissues, it generated good fluorescent signals in stomata (Fig. 1), perhaps useful for stomata functional studies.

By contrast to Arabidopsis, the use of rice tubulin subunits did not label microtubules well *in planta* (Fig. 1B), and caused phenotypic deviations from wild type. Other proteins, such as Lifeact, mTalin and KMD etc. (Kost et al., 1998; Vidali et al. 2009; Deeks et al., 2010), can also be tested as potential rice cytoskeleton labelling strategies.

While we observed nice cytoskeletal fluorescence in developing pollen, we did not observe any signals in pollen mother cells (Fig. S2). It is plausible that this is because the cytoskeleton is too diffuse to be observed reliably with our markers. In future studies, it might be worthwhile to test meiosis-specific promoters to drive fABD/MAP4 to study early rice pollen development, since many rice male sterile-related events are determined at the early microspore stages (Wang et al., 2017; Zhang et al., 2019). Currently, cytoskeleton studies in pollen are mainly focused on pollen germination and pollen tube growth (Chang and Huang, 2015; Liu et al., 2018). By contrast, cytoskeletal function and organization are understudied during pollen grain development. Here, we recorded this process and found that both actin filaments and microtubules change from a disordered to ordered organization (Fig. 3). We note that previous studies did not report the highly ordered/radial microtubule structure that we observed (Zee and Ye, 2000). It is worth noting, that this study used immunelabelling to visualize the microtubules. It is therefore possible that certain developmental stages were missed or that the fixation and staining process damaged the structure, as we found it to be sensitive to stresses (Fig. 4G and S3). Such differences highlight the advantages of live cell imaging that more accurately capture the “natural” state of the cytoskeleton.

The interplay between the actin and microtubule cytoskeleton has been a longstanding research topic in animal cells (Dogterom and Koenderink, 2019). In plant cells, scientists have speculated that the two cytoskeletal polymers interact to fulfill cellular activities (Petrasek and Schwarzerova, 2009). Indeed, several proteins have the ability to associate with both actin and microtubules (Zhang et al., 2011; Sun et al., 2017). In addition, repolymerization of actin filaments occurred along microtubules in Arabidopsis cells (Sampathkumar et al., 2011). The tight co-

alignment of actin bundles and microtubules in maturing rice pollen that we observed (Fig. 4A-E) adds to our understanding of these connections. Here, we found that the actin filaments are necessary to maintain radial microtubule distribution and that the microtubules are essential for actin bundle formation (Fig. 4F, G). Nevertheless, the proteins that facilitate these interactions and the biological function of the radial patterns remain to be addressed.

Soil salinization is a severe agricultural problem in crop production (Mukhopadhyay et al., 2021). Microtubules play an important role in the plant salt tolerance (Chun et al., 2021), and the response of the microtubules to salt has been well documented in Arabidopsis (Wang et al., 2007; Endler et al., 2015). We report a similar response of microtubules during salt stress in rice roots, including depolymerization and subsequent reassembly (Fig. 7A; Table S2). However, we also observed that the re-assembly of microtubules appear to be generated via microtubule-related foci (Fig. 7A; Table 1). We speculate that these foci may act as temporary microtubule "reserves" to recover the microtubule array. Consistent with this, the foci appeared to be guided by the actin cytoskeleton (Fig. 7B, D), a notion supported by actin cytoskeleton depolymerization, which caused significant delay in microtubule recovery (Fig. 7C, E). This emphasizes an important function of the actin cytoskeleton during salt stress. The intact actin cytoskeleton may also be important to maintain cell activity, such as trafficking, during salt exposure. To sum up, by using live cell imaging of actin and microtubule dual labelled lines, combined with drug treatment, we found that actin filaments support the formation and separation of microtubule-related foci during salt exposure (Fig. 7E-H), important for microtubule recovery. Consistently, several actin-associated proteins positively regulate salt tolerance (Zhao et al., 2013; Sengupta et al., 2019; Wang et al., 2021).

Taken together, we generated rice cytoskeleton fluorescent markers and convincingly show that live cell imaging of the cytoskeletal components in rice may provide new insights into the function of some of the most important polymers in plant cell biology and development.

Materials and Methods

Plasmid constructs

All plasmids generated for this publication are based on the vector pCAMBIA1301. For the 35S driven plasmid, the *GFP* was inserted at *Nco* I site and the *fABD/MAP4* was inserted between *Bgl* II and *BstE* II sites. For the *Ubi1* driven GFP lines, *Ubi1* and *GFP* were inserted at *EcoR* I and *Kpn* I site respectively; the *OsfABD/OsTUA1* was inserted between *Hind* III and *Pm* II sites. For other plasmids, the promoters, *Ubi1* or *RUBQ*, were inserted at *EcoR* I site; the fluorescent proteins, *mNeonGreen or mScarlet,* were inserted between *Kpn* I and *BamH* I sites; and the *fABD/MAP4* was inserted between *BamH* I and *BstE* II sites.

The promoter *Ubi* and *RUBQ* were amplified from the vector of pTCK303 (Wang et al., 2004) and pRGEB3.2 (Xie et al., 2015). The fluorescent proteins *mNeonGreen* and *mScarlet* were bought from Allele Biotechnology and Pharmaceuticals (San Diego, USA) (Shaner et al., 2013; Bindels et al., 2017). The *AtfABD* and *MAP4* were amplified from the Arabidopsis seedlings of *35S::GFP-fABD* (Sheahan et al., 2004) and *35S::mCherry-MAP4* (Gutierrez et al., 2009), respectively. The *OsfABD* (LOC_Os02g48740) and *OsTUA1* (LOC_Os03g51600) were amplified from rice cDNA. All the amplification primers are included in Table S4.

The plasmids were transformed into rice calli (*Oryza sativa* Japonica, cultivar 9522) by Agro-infiltration. Transgenic plants were obtained through the skilled technology as reported before in our lab (Cao et al., 2020).

Plant growth conditions

To germinate the seeds, glass petri dishes were used with a layer of filter paper placed at bottom. No more than 50 seeds were put on the paper and deionized water was added until the seeds were just covered. The petri dish was then put into a Percival (E-36L2, Percival Scientific, Iowa, USA) growth chamber (condition:16 h light/8 h dark and 28 ^{o}C/23 ^{o}C) for germination. Aluminum foil was used to cover the petri dish to induce etiolated coleoptiles. After 4 days germination, the seeds were used for coleoptile imaging. After germinating for 5 days, the seedlings were

transferred into liquid 1/2 MS medium for further growth in a black box with a black cover. The cover has small holes to hold the seedlings, letting roots grow into the liquid. These roots were used for imaging. To get adult plants, the rice seedlings were grown in the growth chamber for about one month and then transferred to soil. In the summer the adult rice plants were grown in the field and in the winter they were grown in a greenhouse until flowering and seeds setting.

Sample preparation

For normal imaging, the tissues were usually detached from the entire seedling/plant and the epidermis was imaged. Young stem at tillering stage was sliced into 0.5 cm^2 piece with 1 mm thickness. The epidermis ~0.5 cm^2 was taken by tweezers from coleoptile and leaf grown less than 10 days. 0.5-1 cm length root tips were imaged at indicated age in each particular experiment. Anthers were removed from spikelet and directly mounted without any process. The pollen preparation will be described at next section.

A 3 mm thick special metal holder slide, with a round hole (diameter 1.5 cm) in middle, was used to mount the samples. During the imaging, the samples were placed in the hole held by a cover slide stuck at one side of the metal slide. A prepared round agar pad was used to cover the samples.

Pollen imaging preparation

To image pollens, the preparation was slightly modified. One drop of water (about 20 µl) was kept at the hole place on the cover slide stuck at the bottom side of the metal slide. Anthers from one spikelet were taken into the water and then the anthers were repeatedly squeezed using a tweezer, by which pollens were released into the water. The anther residue was removed. Then another cover slide was stuck on the top of the metal slide without direct touch to the pollen samples, making a free zoom in between and protecting the water evaporation.

For the drug treatment, the water was containing 1 μM oryzalin (19044-88-3, Sigma-Aldrich) or Latrunculin B (76343-94-7, Sigma-Aldrich). Once the pollens are released into the drug containing water, the treatment is started and the imaging began immediately.

To germinate pollens, the shedding pollens were directed scattered on the solid pollen germination medium (Liu et al., 2018). To image hydrated pollens, the medium containing pollens was directed taken for imaging after minuets. To get pollen tubes, the pollens were incubated on the medium for 1 h at 37 ^{o}C.

Salt treatment and imaging preparation

To do the sodium chloride (NaCl) treatment, rice seedlings grown in the black box for 4-5 days were used. The root part of the seedlings were incubated (80 rpm shaking) in liquid 1/2 MS medium containing 250 mM NaCl (CAS:7647-14-5, Sinoreagent, Shanghai, China). After the indicated incubation times, 0.5-1 cm (from root tip) roots were detached from the seedling and mounted on the slide with the NaCl containing medium. The epidermis of roots were imaged

Live cell imaging

Unless specified otherwise images in this article were taken with a spinning disk confocal microscope (SpinSR; Olympus, Tokyo, Japan) equipped with the yokogawa CSU-W1 disk (Tokyo, Japan). Both 100x (NA 1.50, oil) and 60x (NA1.35, silicone oil) objectives were used in an Olympus inverted imaging platform IX83 System. The lasers of 488 nm and 561 nm were used to excite the mNeongreen/GFP and mScarlet proteins, and the emission filters were BP 525/50 and BP 617/73 respectively. Unless specific otherwise, z-stacks were acquired with a step size of 0.5 μm. The time intervals of time series are indicated in the according legends.

Image processing and analysis

All images that are shown in this publication were preprocessed in FIJI (Schindelin et al., 2012), which usually included contrast adjustment, background subtraction, and maximum projection (unless indicated otherwise). Image analysis was done using unprocessed maximum projections of the acquired z-stacks. Colocalization tests were done using Fiji plugin JACoP (Bolte and Cordelières, 2006), in which Manders' coefficients and Pearson coefficient were performed. The microtubule related foci were analyzed by Laplace of Gaussian (https://en.wikipedia.org/wiki/Blob_detection).

Quantification of the cytoskeletal organization for both actin and microtubule marker lines were done using Cytoseg2 (Nowak et al., 2020). The algorithm uses graph theory to describe and create a connected graph of the organization of the filaments. From the connected undirected graph, all edges of the networks were extracted and analyzed in MATLAB (Mathworks, Natick, MA) using 4 parameters: (i) The filament bundling in the network, given by the edge capacity (edge intensity normalized by length). (ii) The network alignment in respect to the major cell axis, given by the weighted mean circular angle (Fisher, 1993; Jammalamadaka and SenGupta, 2001; Berens, 2009). (iii) The randomness of the network, given by the weighted circular variance (Berens, 2009). (iv) The perpendicularity of the network, given by the weighted median of all smallest angles between each edge and the major cell axis. For all angle parameters (ii-iv), the edge angles were weighted by the total intensity of each edge.

The extracted data was analyzed by circular statistics (see Fig. S8). Since some networks can show a bimodal distribution (4), all angles were multiplied by 2, before estimating the mean circular angle and dividing the result by 2 (angle doubling; Fisher, 1993). Estimating the correct mean circular angle from these simulated networks only works for directed networks (3-5). Very random networks (1-2) look very similar and since the angle distribution is very uniform, the mean circular angle is not a useful parameter for these networks. Therefore, we introduced the perpendicularity parameter. Here, the smallest angle between each edge and the major cell axis is calculated, restricting all angles to 0°-90°. Then, the weighted

median of these angles is estimated. In order to avoid confusion with the mean circular angle, the resulting weighted median is rescaled from 0°-90° to 0-1. For random networks the perpendicularity will ≈0.5 (1-2), for directed networks with a 45° angle the perpendicularity is also ≈0.5 (3), but for longitudinal oriented networks the value is close to 0 (4) and for perpendicular oriented networks close to 1 (5).

Accession numbers

OsfABD (LOC_Os02g48740); *OsTUA1* (LOC_Os03g51600).

Acknowledgements

We thank Core Facility and Technical Service Center, School of Life Science and Biotechnologies (Shanghai Jiao Tong University, China) for assistance of confocal microscope, Mingjiao Chen (SJTU, China) and Xiaofei Chen (SJTU, China) for the rice callus transformation and transgenic plant selection.

Conflict of interest

The authors declare no conflict of interest.

Author contributions: Z.L., S.P. and D.Z. conceived the original research plans; Z.L., Y.C., W.C. J.Z. and G.H. performed the experiments; Z.L., F.R. and I. Ø. analyzed data; Z.L., F.R., I. Ø., Z.N., W.L., S.P. and D.Z. wrote the manuscript. All authors discussed the results and commented on the manuscript. D.Z. agrees to serve as the author responsible for contact and ensures communication.

Funding information: This work was funded by National Natural Science Foundation of China (31970803, 32130006 and 31701166), China-Germany Mobility Program (M-0141), Startup Fund for Young Researcher at SJTU (AF0800067), SJTU JiRLMDS Joint Research Fund (MDS-JF-2019A05),

China Postdoctoral Science Foundation (Grant no. 2017M621451), 111 Project (B14016), the Villum, NNF, DNRF, and Australian Research Council Discovery Project (25915, 19OC0056076, DNRF155, DP190101941,and DP210100956).

References

Adamowski M, Li L, Friml J (2019) Reorientation of Cortical Microtubule Arrays in the Hypocotyl of Arabidopsis thaliana Is Induced by the Cell Growth Process and Independent of Auxin Signaling. Int J Mol Sci **20**

Antonius C.J. Timmers, Pascal Vallotton, Claudia Heym, Diedrik Menzel (2007) Microtubule dynamics in root hairs of Medicago truncatula. European Journal of Cell Biology, **86** (2): 69-83

Berens P (2009) CircStat: A MATLAB Toolbox for Circular Statistics. Journal of Statistical Software **1:** 1-21

Bindels DS, Haarbosch L, van Weeren L, Postma M, Wiese KE, Mastop M, Aumonier S, Gotthard G, Royant A, Hink MA, Gadella TW, Jr. (2017) mScarlet: a bright monomeric red fluorescent protein for cellular imaging. Nat Methods **14:** 53-56

Bolte S, Cordelières FP (2006) A guided tour into subcellular colocalization analysis in light microscopy. J Microsc **224:** 213-232

Cao Y, Cai W, Chen X, Chen M, Chu J, Liang W, Persson S, Liu Z, Zhang D (2020) Bright Fluorescent Vacuolar Marker Lines Allow Vacuolar Tracing Across Multiple Tissues and Stress Conditions in Rice. Int J Mol Sci **21**

Chan J (2012) Microtubule and cellulose microfibril orientation during plant cell and organ growth. J Microsc **247:** 23-32

Chang M, Huang S (2015) Arabidopsis ACT11 modifies actin turnover to promote pollen germination and maintain the normal rate of tube growth. Plant J **83:** 515-527

Chang S, Ren Z, Liu C, Du P, Li J, Liu Z, Zhang F, Hou H, Shi J, Liang W, Yang L, Ren H, Zhang D. (2021) *OsFH3* Encodes a Type II Formin Required for Rice Morphogenesis. Int J Mol Sci. **22**(24):13250

Chun HJ, Baek D, Jin BJ, Cho HM, Park MS, Lee SH, Lim LH, Cha YJ, Bae DW, Kim ST, Yun DJ, Kim MC (2021) Microtubule Dynamics Plays a Vital Role in Plant Adaptation and Tolerance to Salt Stress. Int J Mol Sci **22**

Courtemanche N, Pollard TD, Chen Q (2016) Avoiding artefacts when counting polymerized actin in live cells with LifeAct fused to fluorescent proteins. Nat Cell Biol **18**(6):676-83.

Deeks M, Fendrych M, Smertenko A, Bell K, Oparka K, Cvrčková F, Žárský V, Hussey P (2010) The plant formin AtFH4 interacts with both actin and microtubules, and contains a newly identified microtubule-binding domain. J Cell Sci **123**(8): 1209–1215.

Dogterom M, Koenderink GH (2019) Actin-microtubule crosstalk in cell biology. Nat Rev Mol Cell Biol **20:** 38-54

Endler A, Kesten C, Schneider R, Zhang Y, Ivakov A, Froehlich A, Funke N, Persson S (2015) A Mechanism for Sustained Cellulose Synthesis during Salt Stress. Cell **162:** 1353-1364

Fisher NI (1993) Statistical Analysis of Circular Data. Cambridge University Press, Cambridge

Flores LR, Keeling MC, Zhang X, Sliogeryte K, Gavara N (2019) Lifeact-GFP alters F-actin organization, cellular morphology and biophysical behaviour. Sci Rep **9**(1):3241

Gutierrez R, Lindeboom JJ, Paredez AR, Emons AM, Ehrhardt DW (2009) Arabidopsis cortical microtubules position cellulose synthase delivery to the plasma membrane and interact with cellulose synthase trafficking compartments. Nat Cell Biol **11:** 797-806

Huang G, Liang W, Sturrock CJ, Pandey BK, Giri J, Mairhofer S, Wang D, Muller L, Tan H, York LM, Yang J, Song Y, Kim YJ, Qiao Y, Xu J, Kepinski S, Bennett MJ, Zhang D. (2018) Rice actin binding protein RMD controls crown root angle in response to external phosphate. Nat Commun **9**(1):2346

Jammalamadaka SR, SenGupta A (2001) Topics in Circular Statistics, Vol Volume 5. WORLD SCIENTIFIC

Komorisono M, Ueguchi-Tanaka M, Aichi I, Hasegawa Y, Ashikari M, Kitano H, Matsuoka M, Sazuka T (2005) Analysis of the rice mutant dwarf and gladius leaf 1. Aberrant katanin-mediated microtubule organization causes up-regulation of gibberellin biosynthetic genes independently of gibberellin signaling. Plant Physiol **138:** 1982-1993

Kost B, Mathur J, Chua NH (1999) Cytoskeleton in plant development. Curr Opin Plant Biol **2:** 462-470

Kost B, Spielhofer P, Chua NH (1998) A GFP-mouse talin fusion protein labels plant actin filaments in vivo and visualizes the actin cytoskeleton in growing pollen tubes. Plant J **16:** 393-401

Li G, Liang W, Zhang X, Ren H, Hu J, Bennett MJ, Zhang D. (2014) Rice actin-binding protein RMD is a key link in the auxin-actin regulatory loop that controls cell growth. Proc Natl Acad Sci U S A. **111**(28):10377-82

Lipka E, Herrmann A, Mueller S (2015) Mechanisms of plant cell division. Wiley Interdiscip Rev Dev Biol **4:** 391-405

Liu C, Zhang Y, Ren H (2018) Actin Polymerization Mediated by AtFH5 Directs the Polarity Establishment and Vesicle Trafficking for Pollen Germination in Arabidopsis. Mol Plant **11:** 1389-1399

Lo SF, Cheng ML, Hsing YC, Chen YS, Lee KW, Hong YF, Hsiao Y, Hsiao AS, Chen PJ, Wong LI, Chen NC, Reuzeau C, Ho TD, Yu SM (2020) Rice Big Grain 1 promotes cell division to enhance organ development, stress tolerance and grain yield. Plant Biotechnol J **18:** 1969-1983

Maeda K, Higaki T (2021) Disruption of actin filaments delays accumulation of cell plate membranes after chromosome separation. Plant Signal Behav **16:** 1873586

Maeda K, Sasabe M, Hanamata S, Machida Y, Hasezawa S, Higaki T (2020) Actin Filament Disruption Alters Phragmoplast Microtubule Dynamics during the Initial Phase of Plant Cytokinesis. Plant Cell Physiol **61:** 445-456

Marc J, Granger CL, Brincat J, Fisher DD, Kao T, McCubbin AG, Cyr RJ (1998) A GFP-MAP4 reporter gene for visualizing cortical microtubule rearrangements in living epidermal cells. Plant Cell **10:** 1927-1940

Mohanty A, Luo A, DeBlasio S, Ling X, Yang Y, Tuthill DE, Williams KE, Hill D, Zadrozny T, Chan A, Sylvester AW, Jackson D (2009) Advancing cell biology and functional genomics in maize using fluorescent protein-tagged lines. Plant Physiol **149**(2):601-5

Mukhopadhyay R, Sarkar B, Jat HS, Sharma PC, Bolan NS (2021) Soil salinity under climate change: Challenges for sustainable agriculture and food security. J Environ Manage **280:** 111736

Nowak J, Gennermann K, Persson S, Nikoloski Z (2020) CytoSeg 2.0: automated extraction of actin filaments. Bioinformatics **36:** 2950-2951

Panteris E (2008) Cortical actin filaments at the division site of mitotic plant cells: a reconsideration of the 'actin-depleted zone'. New Phytol **179:** 334-341

Petrasek J, Schwarzerova K (2009) Actin and microtubule cytoskeleton interactions. Curr Opin Plant Biol **12:** 728-734

Qu X, Zhang R, Zhang M, Diao M, Xue Y, Huang S (2017) Organizational Innovation of Apical Actin Filaments Drives Rapid Pollen Tube Growth and Turning. Mol Plant **10:** 930-947

Sampathkumar A, Lindeboom JJ, Debolt S, Gutierrez R, Ehrhardt DW, Ketelaar T, Persson S (2011) Live cell imaging reveals structural associations between the actin and microtubule cytoskeleton in Arabidopsis. Plant Cell **23:** 2302-2313

Schindelin J, Arganda-Carreras I, Frise E, Kaynig V, Longair M, Pietzsch T, Preibisch S, Rueden C, Saalfeld S, Schmid B, Tinevez JY, White DJ, Hartenstein V, Eliceiri K, Tomancak P, Cardona A (2012) Fiji: an open-source platform for biological-image analysis. Nat Methods **9:** 676-682

Seck PA, Diagne A, Mohanty S, Wopereis MCS (2012) Crops that feed the world 7: Rice. Food Security **4:** 7-24

Sengupta S, Mangu V, Sanchez L, Bedre R, Joshi R, Rajasekaran K, Baisakh N (2019) An actin-depolymerizing factor from the halophyte smooth cordgrass, Spartina alterniflora (SaADF2), is superior to its rice homolog (OsADF2) in conferring drought and salt tolerance when constitutively overexpressed in rice. Plant Biotechnol J **17:** 188-205

Shaner NC, Lambert GG, Chammas A, Ni Y, Cranfill PJ, Baird MA, Sell BR, Allen JR, Day RN, Israelsson M, Davidson MW, Wang J (2013) A bright monomeric green fluorescent protein derived from Branchiostoma lanceolatum. Nat Methods **10:** 407-409

Shaw SL, Kamyar R, Ehrhardt DW (2003) Sustained Microtubule Treadmilling in Arabidopsis Cortical Arrays. Science **300:** 1715-1718

Sheahan MB, Staiger CJ, Rose RJ, McCurdy DW (2004) A green fluorescent protein fusion to actin-binding domain 2 of Arabidopsis fimbrin highlights new features of a dynamic actin cytoskeleton in live plant cells. Plant Physiol **136:** 3968-3978

Sikora J, Wasik A, Zajaczkowska M (1991) Cytoplasmic streaming direction reverses in dividing Paramecium bursaria. Eur J Protistol **27**(4):352-6

Song Y, Li G, Nowak J, Zhang X, Xu D, Yang X, Huang G, Liang W, Yang L, Wang C, Bulone V, Nikoloski Z, Hu J, Persson S, Zhang D (2019) The Rice Actin-Binding Protein RMD Regulates Light-Dependent Shoot Gravitropism. Plant Physiol **181:** 630-644

Sun T, Li S, Ren H (2017) OsFH15, a class I formin, interacts with microfilaments and microtubules to regulate grain size via affecting cell expansion in rice. Sci Rep **7:** 6538

Ueda K, Matsuyama T, Hashimoto T (1999) Visualization of microtubules in living cells of transgenic *Arabidopsis thaliana*. Protoplasma **206:** 201–206

Vidali L, Rounds CM, Hepler PK, Bezanilla M (2009) Lifeact-mEGFP reveals a dynamic apical F-actin network in tip growing plant cells. PLoS One **4**(5):e5744

Wang C, Li J, Yuan M (2007) Salt Tolerance Requires Cortical Microtubule Reorganization in Arabidopsis, Plant and Cell Physiology **11:** 1534–1547

Wang C, Higgins JD, He Y, Lu P, Zhang D, Liang W (2017) Resolvase OsGEN1 Mediates DNA Repair by Homologous Recombination. Plant Physiol **173:** 1316-1329

Wang L, Qiu T, Yue J, Guo N, He Y, Han X, Wang Q, Jia P, Wang H, Li M, Wang C, Wang X (2021) Arabidopsis ADF1 Regulated by MYB73 is Involved in Response to Salt Stress via Affecting Actin Filaments Organization. Plant Cell Physiol

Wang M, Chen C, Xu YY, Jiang RX, Han Y, Xu ZH, Chong K (2004) A practical vector for efficient knockdown of gene expression in rice (Oryza sativa L.). Plant Molecular Biology Reporter **22:** 409-417

Wang X, Mao T (2019) Understanding the functions and mechanisms of plant cytoskeleton in response to environmental signals. Curr Opin Plant Biol **52:** 86-96

Xie K, Minkenberg B, Yang Y (2015) Boosting CRISPR/Cas9 multiplex editing capability with the endogenous tRNA-processing system. Proc Natl Acad Sci U S A **112:** 3570-3575

Xu XL, Walter WJ, Liu Q, Machens I, Nick P (2018) A rice class-XIV kinesin enters the nucleus in response to cold. Scientific Reports **8**

Yang BJ, Wendrich JR, De Rybel B, Weijers D, Xue HW (2020) Rice microtubule-associated protein IQ67-DOMAIN14 regulates grain shape by modulating microtubule cytoskeleton dynamics. Plant Biotechnology Journal **18:** 1141-1152

Yu Y, Wu S, Nowak J, Wang G, Han L, Feng Z, Mendrinna A, Ma Y, Wang H, Zhang X, Tian J, Dong L, Nikoloski Z, Persson S, Kong Z (2019) Live-cell imaging of the cytoskeleton in elongating cotton fibres. Nat Plants **5:** 498-504

Zee SY, Ye XL (2000) Microtubule reorganization during pollen development of rice (Oryza sativa L.). Protoplasma **210:** 188-201

Zhang J, Wang C, Higgins JD, Kim YJ, Moon S, Jung KH, Qu S, Liang W (2019) A Multiprotein Complex Regulates Interference-Sensitive Crossover Formation in Rice. Plant Physiol **181:** 221-235

Zhang M, Zhang B, Qian Q, Yu Y, Li R, Zhang J, Liu X, Zeng D, Li J, Zhou Y (2010) Brittle Culm 12, a dual-targeting kinesin-4 protein, controls cell-cycle progression and wall properties in rice. Plant J **63:** 312-328

Zhang Z, Zhang Y, Tan H, Wang Y, Li G, Liang W, Yuan Z, Hu J, Ren H, Zhang D (2011) RICE MORPHOLOGY DETERMINANT encodes the type II formin FH5 and regulates rice morphogenesis. Plant Cell **23:** 681-700

Zhao Y, Pan Z, Zhang Y, Qu X, Zhang Y, Yang Y, Jiang X, Huang S, Yuan M, Schumaker KS, Guo Y (2013) The actin-related Protein2/3 complex regulates mitochondrial-associated calcium signaling during salt stress in Arabidopsis. Plant Cell. **25**(11):4544-59

Figures and Table

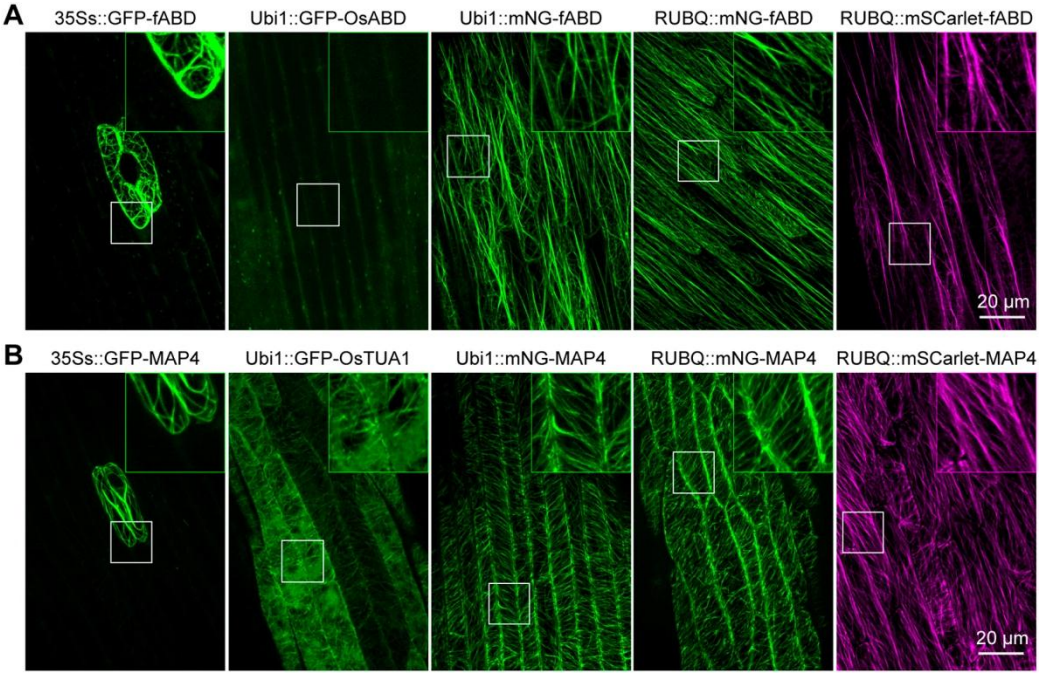

Figure 1. The comparison of different rice cytoskeleton marker lines. (A) Actin and (B) microtubule cytoskeleton markers in transgenic rice coleoptile. Epidermis of coleoptiles, germinated for 3.5 days, were used for the imaging. The images are maximum-projections from z-stack series. The white rectangles indicate the regions for each enlargement at the upper right corner in each big image. The yellow arrow heads indicate cells with silenced signals and the white arrow heads indicate cytosolic signals.

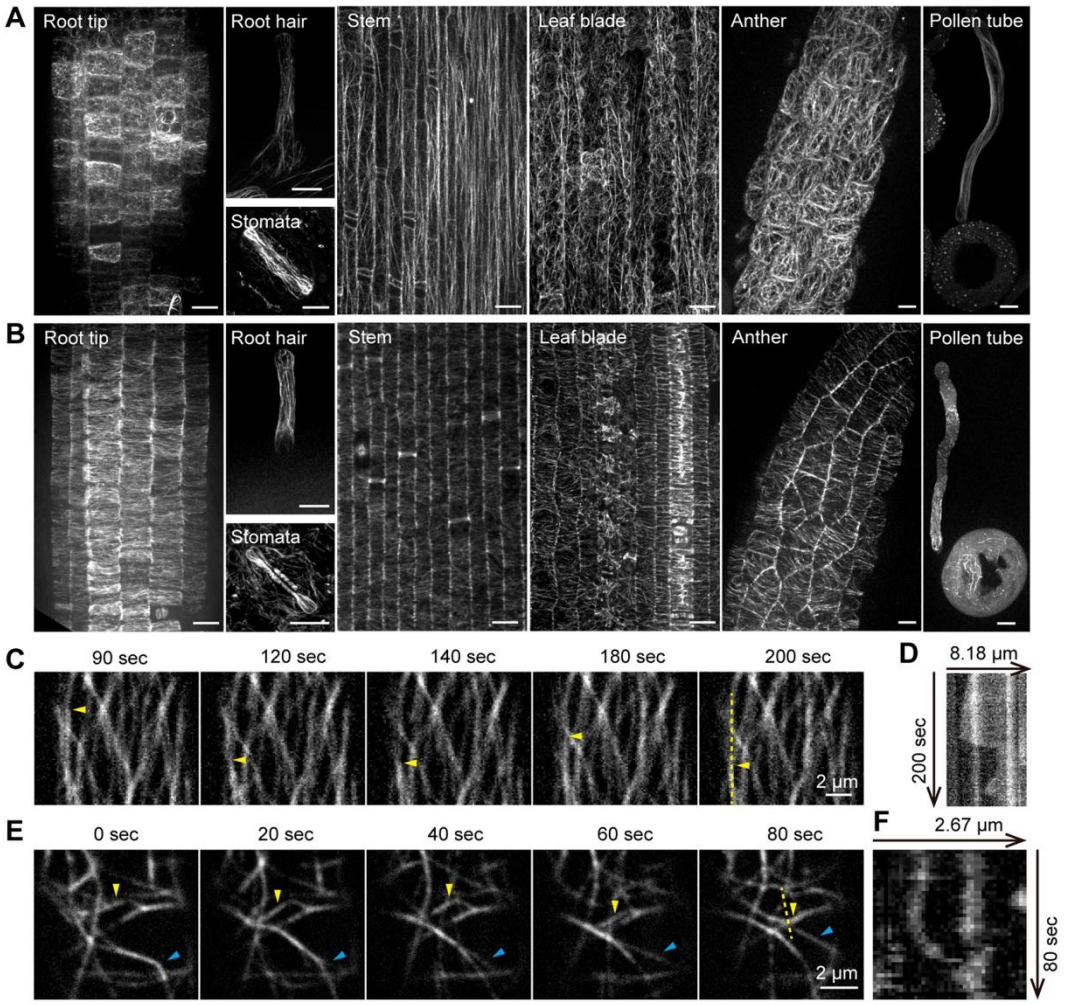

Figure 2. Cytoskeletal patterns and behavior in different rice tissues using live-cell imaging of fluorescent marker lines. (A) Example images of actin cytoskeleton in different rice tissues, including vegetative cells and reproductive cells. All images are maximum projected and obtained from the actin lines *RUBQ::mNG-fABD* (mNG-fABD). Scale bars: 10 μm. (B) Example images of microtubules in different rice tissues. The images of the root tip and root hair were obtained from *RUBQ::mScarlet-MAP4* (mScarlet-MAP4 hereafter) lines and the rest were all from the *RUBQ::mNG-MAP4* (mNG-MAP4) line. All images are maximum projected. Scale bars: 10 μm. (C) A time series of mNG-MAP4 in root with 2 sec time interval. The yellow arrows are following a microtubule end. (D) Kymograph following microtubule catastrophe and rescue. The position is indicated by the dashed line in (C). (E) A time series of mNG-fABD in root with 2 sec time interval. The yellow and cyan arrows are following a bundling and unbundling actin filament and bundle, respectively. (F) Kymograph following the bundling actin event at position indicated by the dashed line in (E).

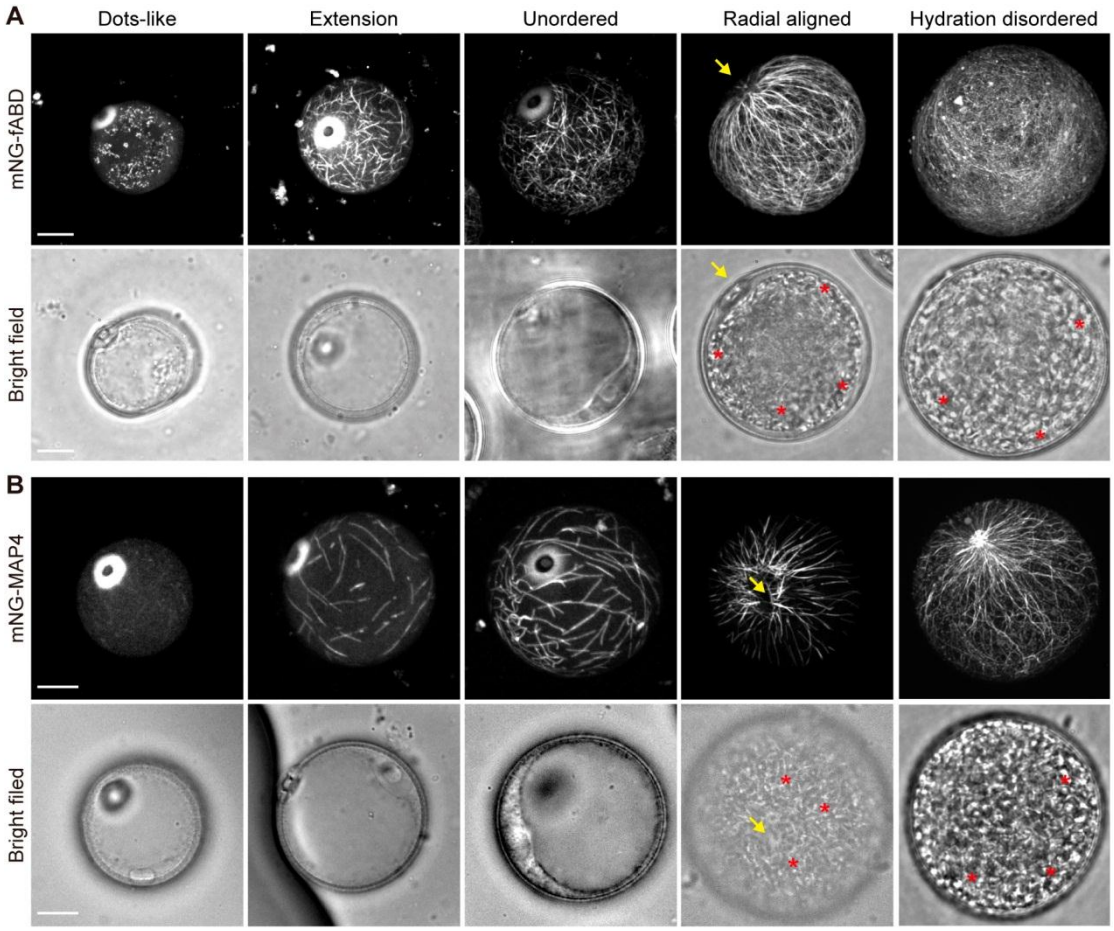

Figure 3. Organizational changes in the cytoskeleton during rice pollen development. (A) Actin filament organization in different pollen developmental stages. (B) Microtubule organization in different pollen developmental stages. The fluorescent channels are maximum projections of z-stacks. The bright field channels are a single focal plane selected from z-stacks to show the size of the pollen. The diameter increase (from left to right) of the pollen grains indicates the pollen development from immature to mature. The pollen germination pores are indicated by the yellow arrows. The red asterisks indicate amyloplasts. Scale bars: 10 μm.

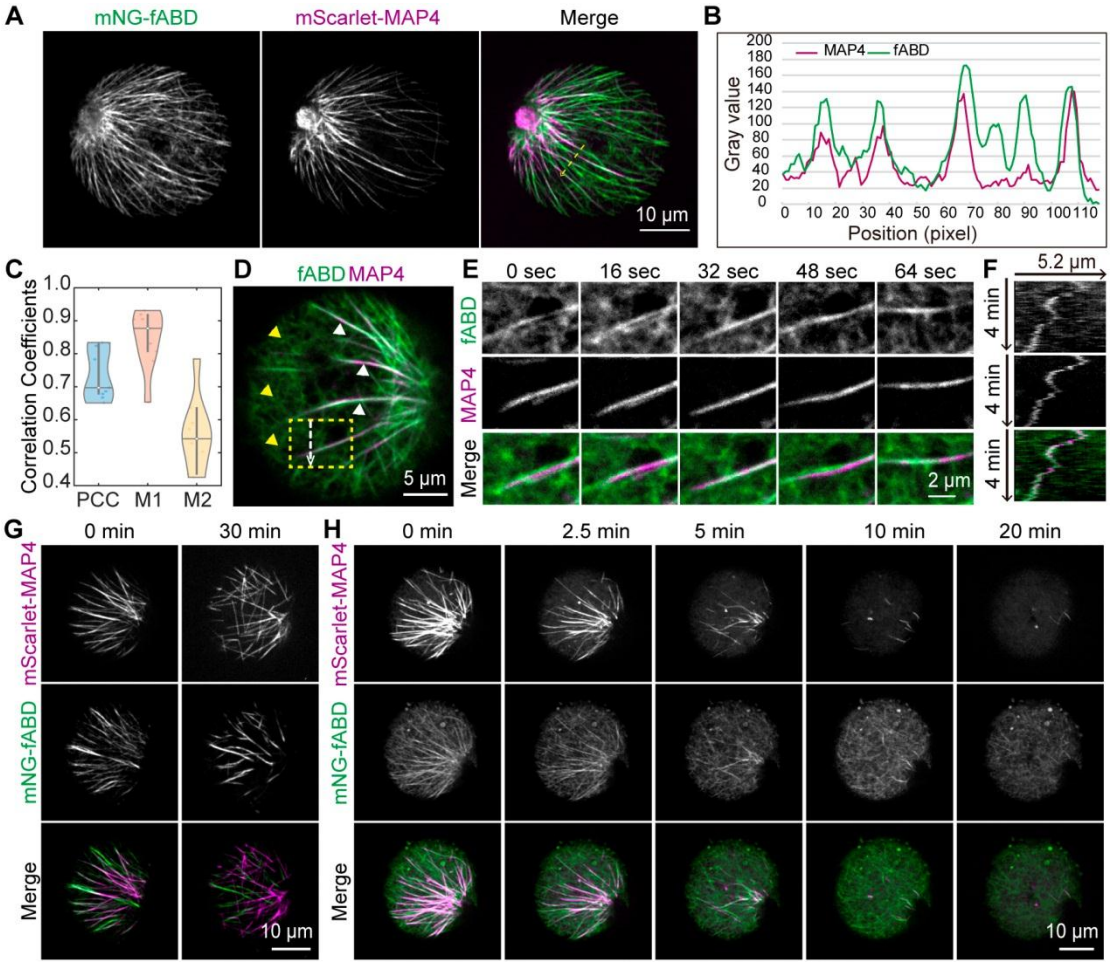

Figure 4. The actin and microtubule cytoskeletons engage with each other during rice pollen development. (A) Colocalization between actin and microtubule cytoskeletons in maturing rice pollen. Images were taken from the microtubule and actin dual labelled line *RUBQ::mScarlet-MAP4 RUBQ::mNG-fABD*. (B) Line plot of the position of the yellow dashed line in (A). (C) Correlation coefficients between filamentous actin and microtubule fluorescence in pollens. PCC means Pearson correlation coefficient. Mander's coefficient test was used for M1 (the fraction of mScarlet-MAP4 on mNG-fABD) and M2 (the fraction of mNG-fABD on mScarlet-MAP4). n= 10 pollens. (D) Representative image of a rice pollen showing partial colocalization between filamentous actin and microtubules. The white arrow heads indicate actin bundles and yellow arrow heads indicate fine actin filaments, which show low colocalization with microtubules. (E) A time series showing association between actin bundles and microtubules as they migrate. The imaged region was from the yellow rectangle in (D), with a time interval of 4 sec. (F) Kymographs showing the co-migration between actin bundle (upper panel) and microtubule (middle panel). Kymograph line is indicated by the white dashed arrow in (D). (G) Treatment of rice pollen with 1 μM actin inhibitor Latrunculin B. The decreased abundance of filamentous actin after the treatment indicates partial actin depolymerization. (H) Treatment of rice pollen with 1 μM microtubule inhibitor oryzalin. Time interval was 0.5 min. The images in (A) (G) (H) are maximum projections while in (D) (E) are single focal frames.

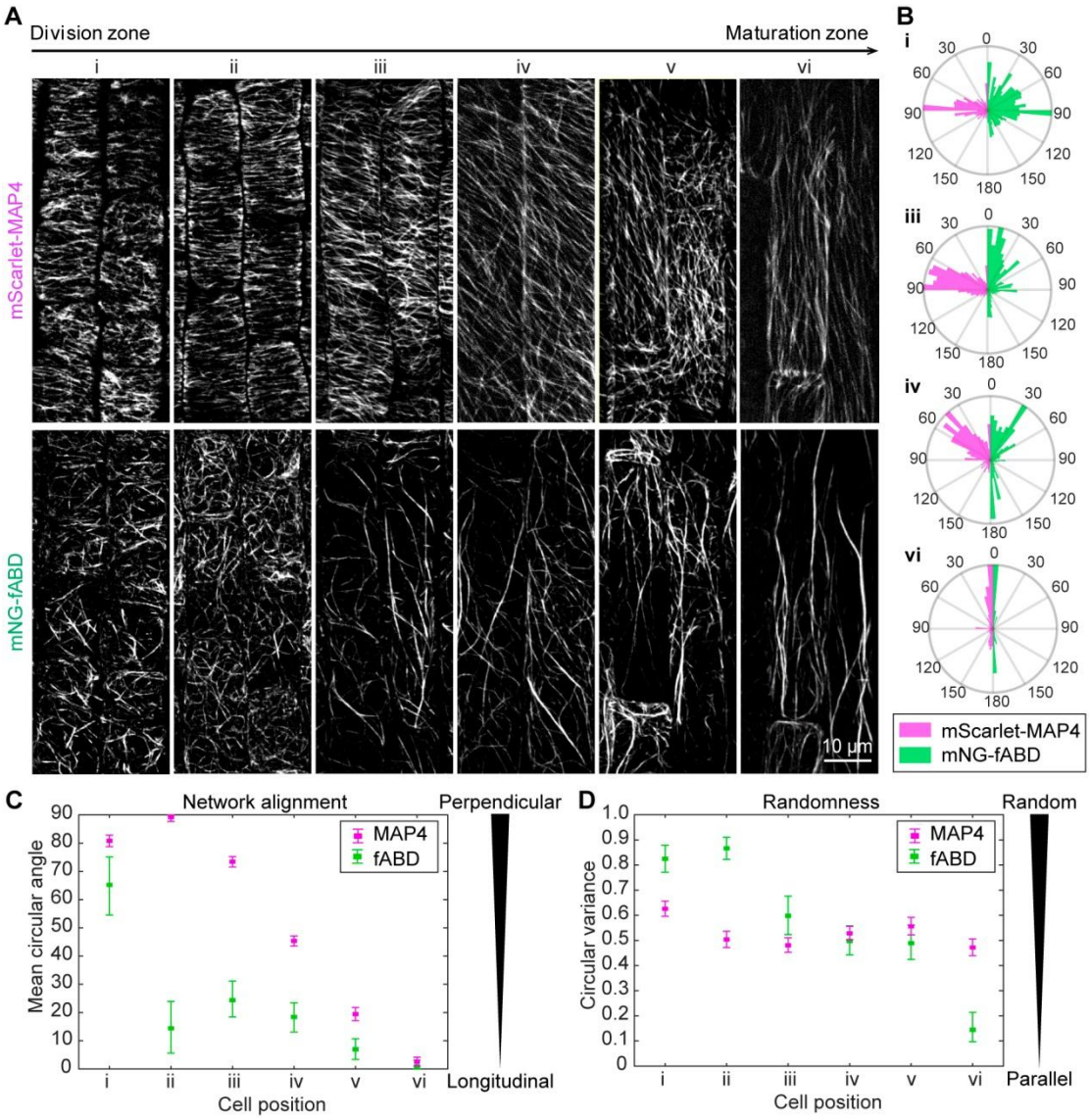

Figure 5. The organization of filamentous actin and microtubules in dividing root cells of rice. The root tips of actin and microtubule dual labelled rice lines were used for the observation. The images are all maximum projections. The filamentous actin signal changes during the preprophase band formation (the upper four panels of mNG-fABD). Yellow arrowhead indicates fine actin filaments associating with the growing cell plate. Scale bar: 5 μm.

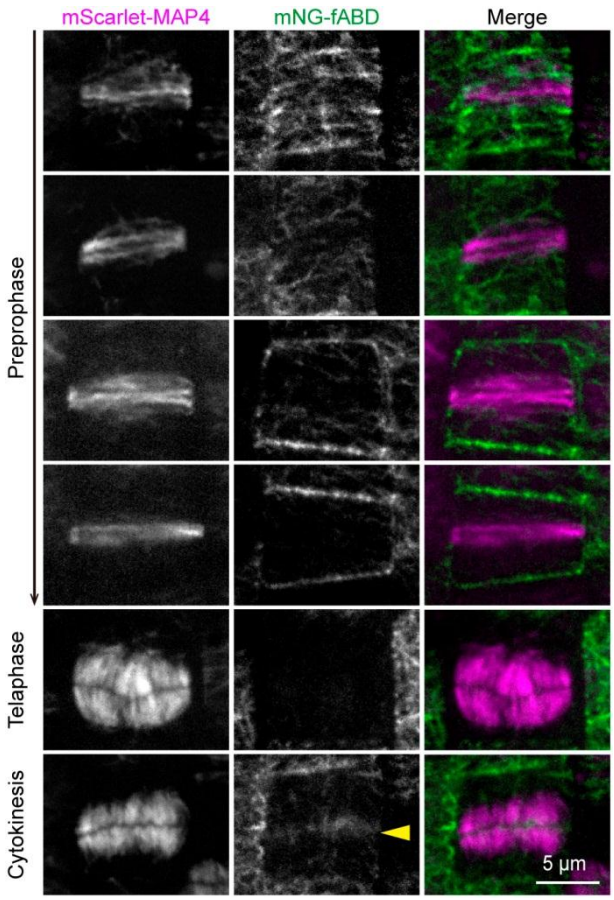

Figure 6. The cytoskeletons reorient in a coordinated fashion during cell growth in rice root. (A) Images tracking cytoskeleton redirection during root cell growth. The images from left to right panels were taken from the root tip region to the maturing region in the dual label line. The images are maximum projected from z-stacks of root epidermal cells. (B) Circular histograms for all edge angles (weighted by edge length) of actin and microtubule cytoskeletons, extracted from selected images in (A) using Cytoseg2.0. The major axis of the cell (longitudinal) is defined as 0°. (C) Quantification of changes in the network alignment for filamentous actin and microtubules from images in (A). Large angles describe a network that is oriented perpendicular to the major cell axis, small angles a longitudinal orientation. (D) Quantification of network randomness for filamentous actin and microtubules from images in (A). Small values describe a network with parallel edges, and large values a wider distribution of edge orientation.

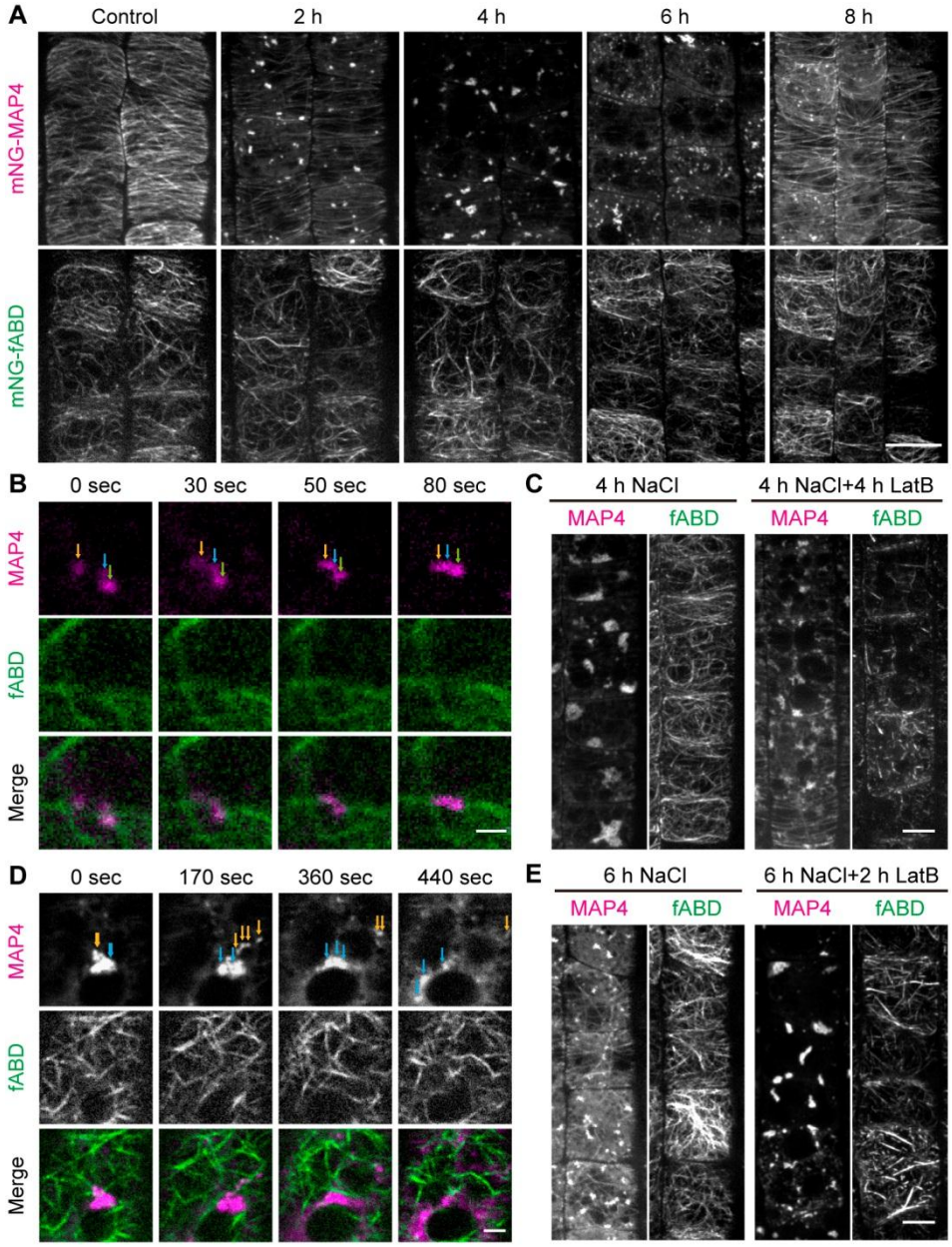

Figure 7. Actin cytoskeleton facilitates microtubule re-emergence upon salt treatment. (A) Actin (mNG-fABD) and microtubule (mScarlet-MAP4) cytoskeleton response to salt treatment. Five-day old seedlings (after crown root emergence) were incubated with 250 mM NaCl containing liquid medium for the indicated time. The epidermal cells of dual labelled lines were imaged by z-scanning. The images of root transition zone (see the definition in Fig. S6) are maximum projected and cropped. Scale bar: 10 μm. (B) Time lapse series to show the merge of microtubule-related foci. Seedlings were incubated with salt for 1.5 h. The arrows are tracking the positions of microtubule-related foci. Scale bar: 1 μm. (C) Microtubule-related foci formation after 4 h salt incubation with or without 0.5 μM Latrunculin B (LatB).

Scale bar: 5 μm. (D) Time lapse series to show the separation of microtubule-related foci. Seedlings were incubated with salt for 5 h. The arrows are tracking the separation of microtubule-related foci. Scale bar: 2 μm. (E) Microtubule-related foci disappearance after 6 h salt incubation with or without LatB. LatB was added at 4 h after salt incubation. Scale bar: 5 μm. Images in both (C) and (E) are maximum projections.

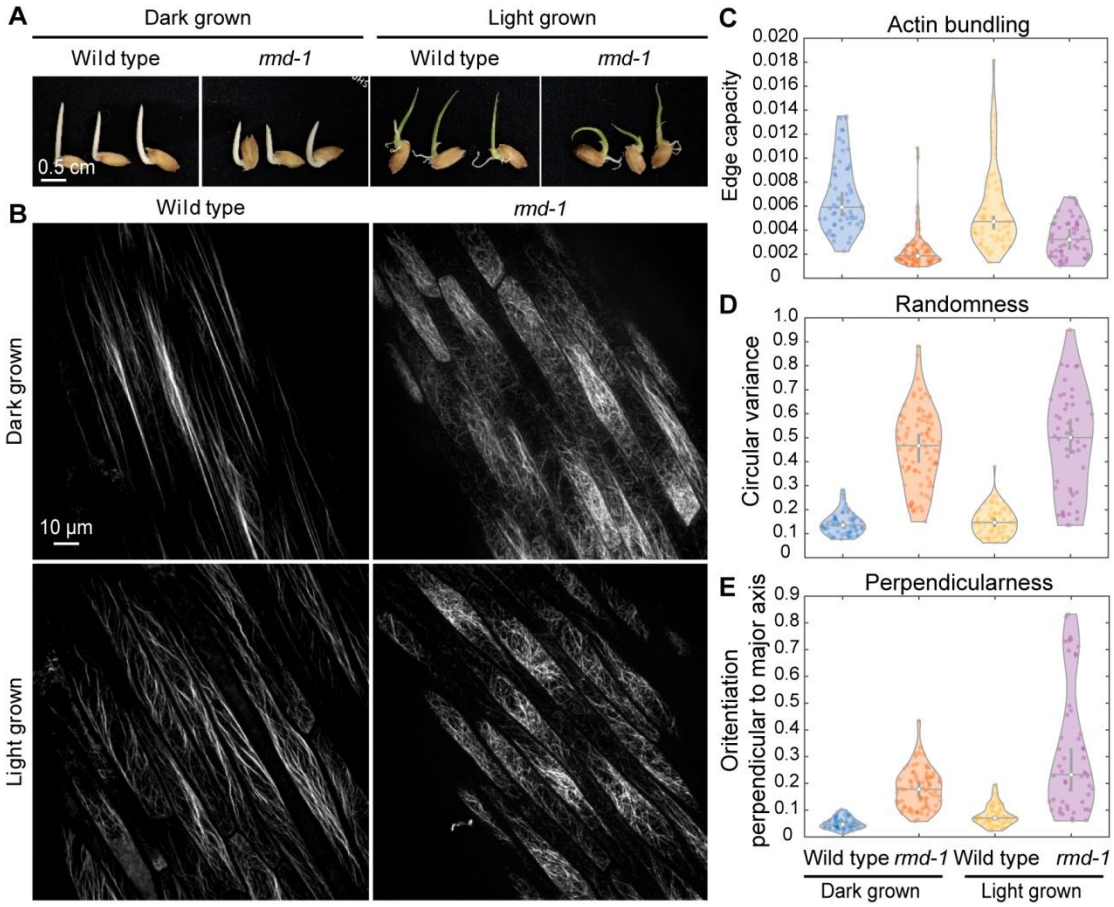

Figure 8. Live cell imaging reveals that RMD supports actin bundling in rice interphase cells. (A) Rice seedlings (wild type and *rmd-1* mutant) were germinated under light and dark, respectively. The seedlings were germinated for 5 days. The crown roots were removed. (B) Maximum projected images of actin cytoskeleton in the epidermis of coleoptiles germinated for 4 days. Note the filamentous actin pattern and distribution in the cells. (C) Quantification of actin bundling in coleoptiles grown in the dark (N=57 cells for wild type and 84 cells for *rmd-1*) and in the light (N=71 cells for wild type and 50 cells for *rmd-1*) of wild type and *rmd-1* mutants using Cytoseg2.0. (D) Quantification of the network randomness for the cells analyzed in (C) (for more details on the circular statistics see Figure S8). (E) Quantification of the network perpendicularity for the cells analyzed in (C).

Table 1. Quantification of microtubule foci after salt treatment, related to Fig. 7A. The seedlings were incubated with 250 mM NaCl for indicated time. Microtubule related foci size (radius in pixel) and number were analyzed by Laplace of Gaussian method. The root transition zones of five seedlings were used for analysis at each time point (See Fig. 7 for other details).

Time point	Median of radius in pixel	Median absolute deviation	Number of cells	Mean number per cell
1.5-2 h	4.07	0.68	96	4.80
3.5-4 h	4.99	1.26	111	8.62
5.5-6 h	2.93	0.89	122	7.35
7.5-8 h	3.64	0.57	138	1.03

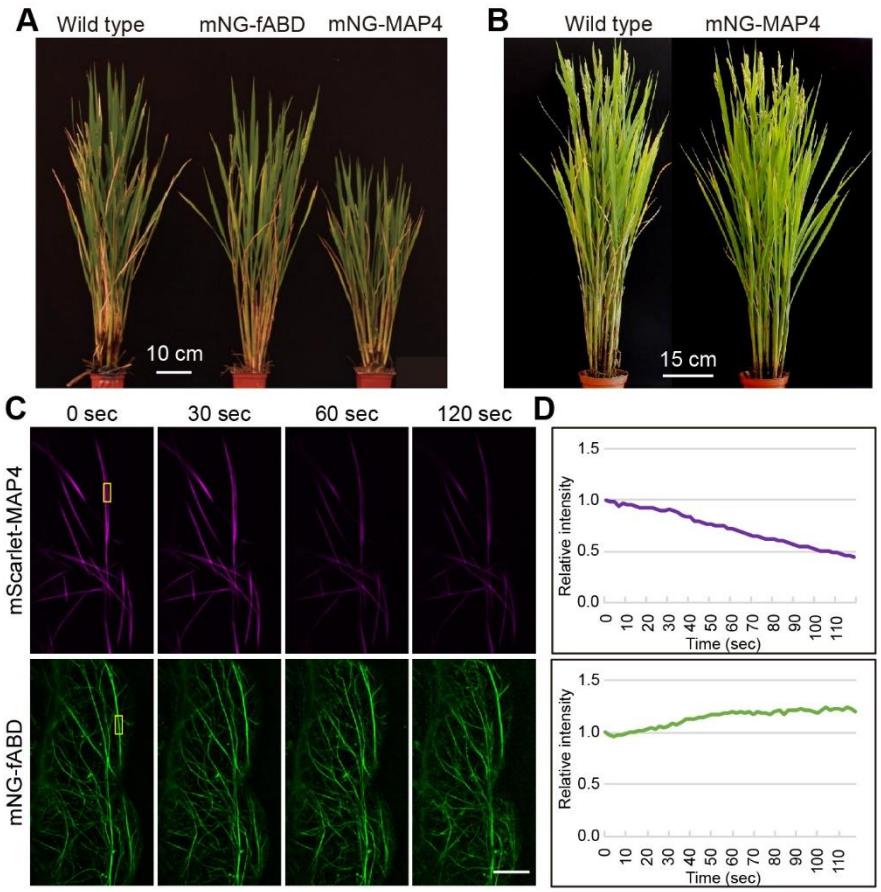

Fig. S1. The plant phenotype and photo-bleaching of RUBQ driving lines. (A-B) The transgenic plant phenotype of *mNG-fABD* and *mNG-MAP4* lines. The *mNG-fABD* lines are indistinguishable from the wild-type plants. Some *mNG-MAP4* lines can cause plant dwarf phenotype (A) while some normal lines as in (B) can also be obtained. (C) Bleaching test for the fluorescent proteins. The images were from a time lapse stack taken from the coleoptile epidermis of dual labelled line *RUBQ2::mScarlet-MAP4 RUBQ2::mNG-fABD (mScarlet-MAP4 mNG-fABD* in short*)*. The duration was 2 min with 2 sec time interval. Note the quick intensity decrease of the mScarlet channel. Scale bar: 10 μm. (D) Fluorescent signal plot of the yellow rectangle regions in (C).

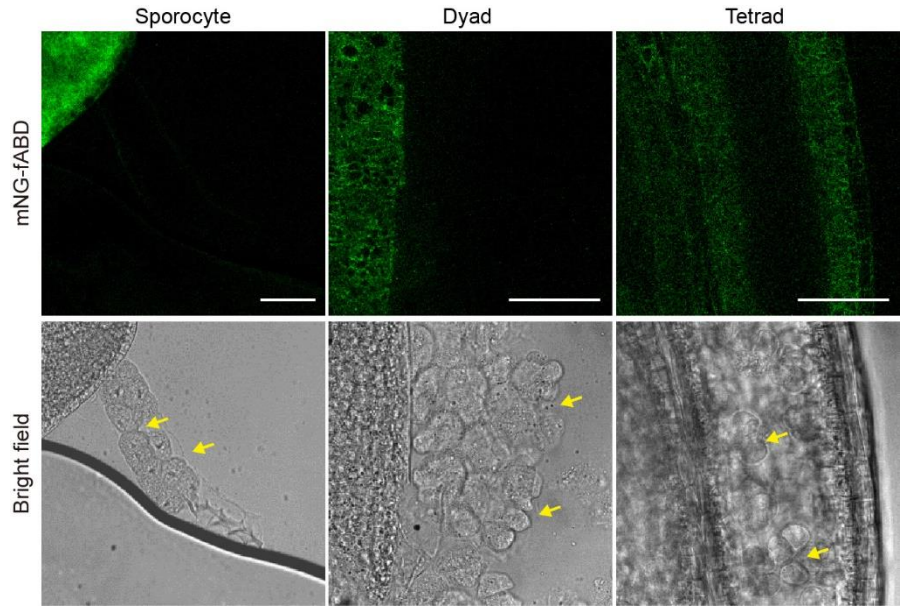

Fig. S2. RUBQ driven actin cytoskeleton signal is absent in pollen mother cells. Single images of young anthers from the mNG-fABD line. Arrows indicate the pollen mother cells where no clear green signals can be seen. Scale bars: 10 μm.

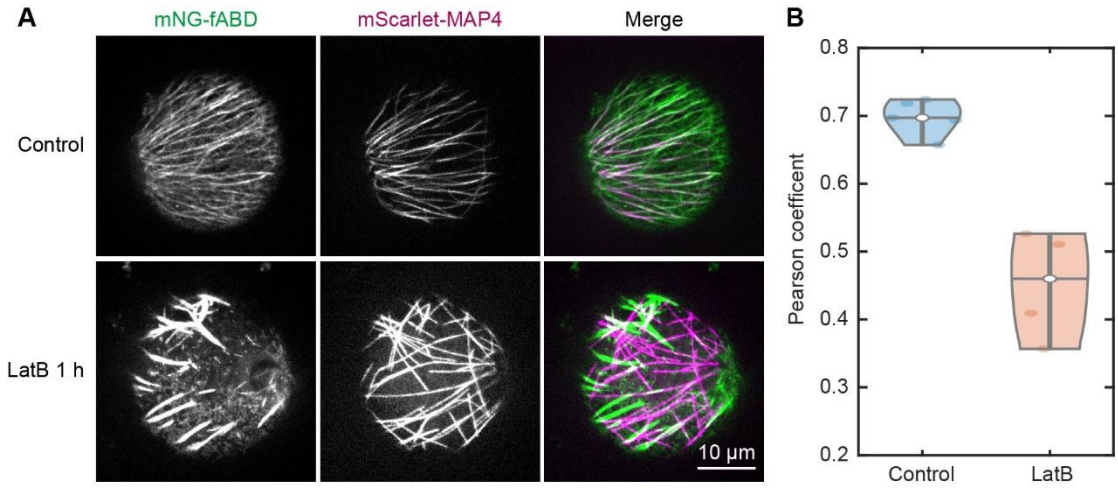

Fig. S3. Partial depolymerization of actin cytoskeleton decreased the interplay between actin and microtubule in rice pollen. (A) Maximum projected images of the cytoskeletons in pollen with/without LatB treatment. The pollen was treated with 1 μM actin inhibitor Latrunculin B for 1 h. Note the change of microtubules from radial alignment to more disordered alignment. (B) Pearson correlation coefficient between actin filaments and microtubules in the treatment in (A). 4 to 5 pollens were used for this analysis.

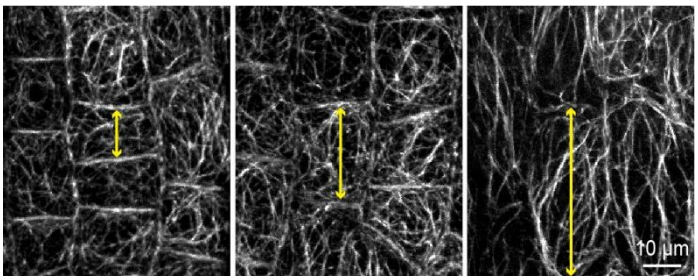

Fig. S4. Actin cytoskeleton reorientation in anther epidermis. Actin filaments in rice anther epidermis where the actin direction changes from disordered to longitudinal (from left to right) alignment. The increased cell length (indicating by yellow arrows) indicates the cell growth stage. The images are maximum projections.

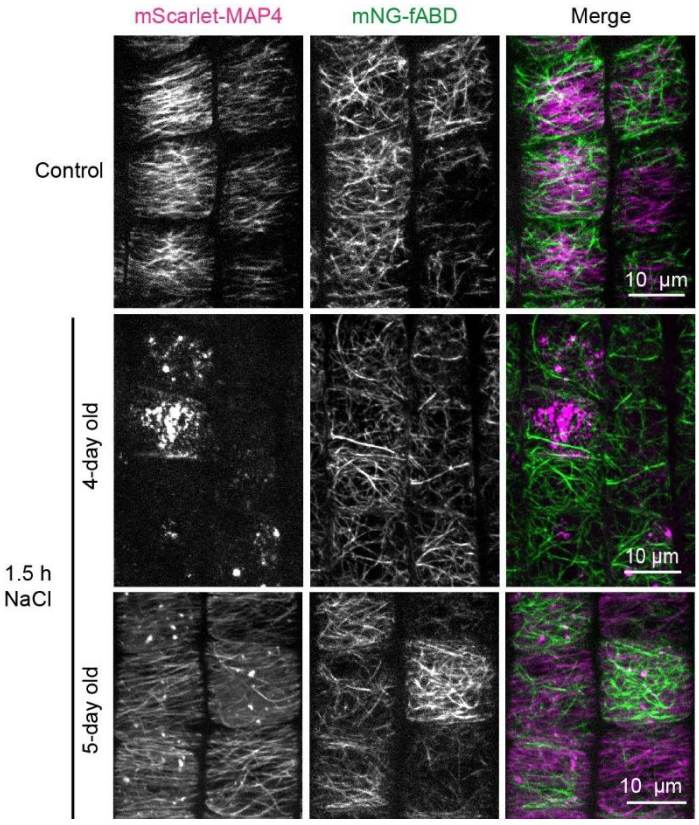

Fig. S5. Seedling age determines the sensitivity to salt treatment. Images of different age rice seedlings were treated with 250 mM NaCl. The images are maximum projections from root epidermis. Note that the difference of microtubule depolymerizing extent and microtubule-related foci number.

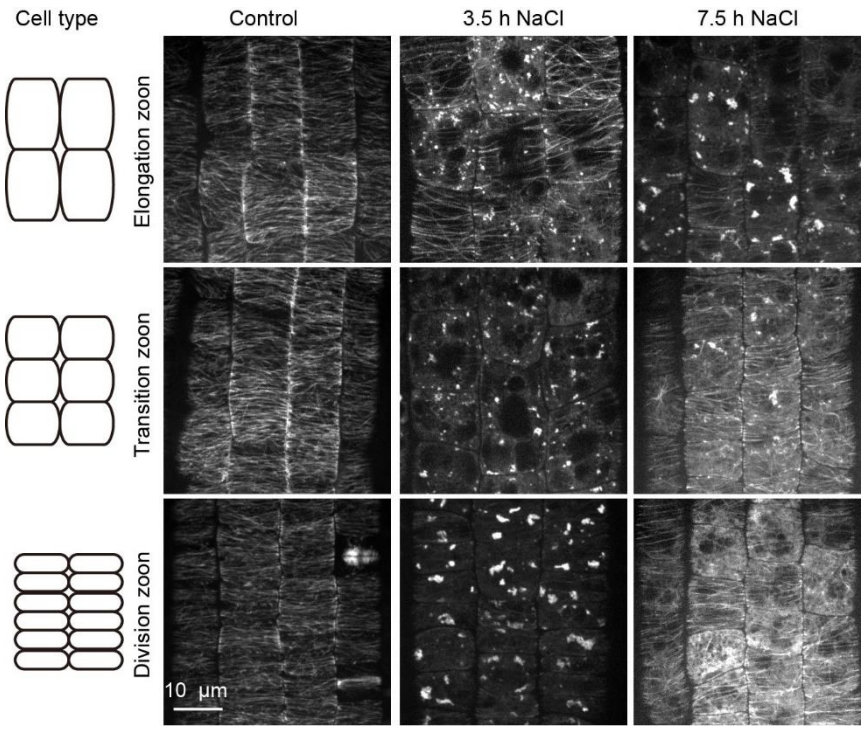

Fig. S6. The timing of microtubule response to salt differs in root cell types. Images of microtubule (mScarlet-MAP4) in different root epidermal cells. Schematic views of the cell shape at different zones are outlined in left panel. The root parts of five-day old seedlings were incubated with 250 mM NaCl for the indicated times. The images are maximum projections from z-stacks.

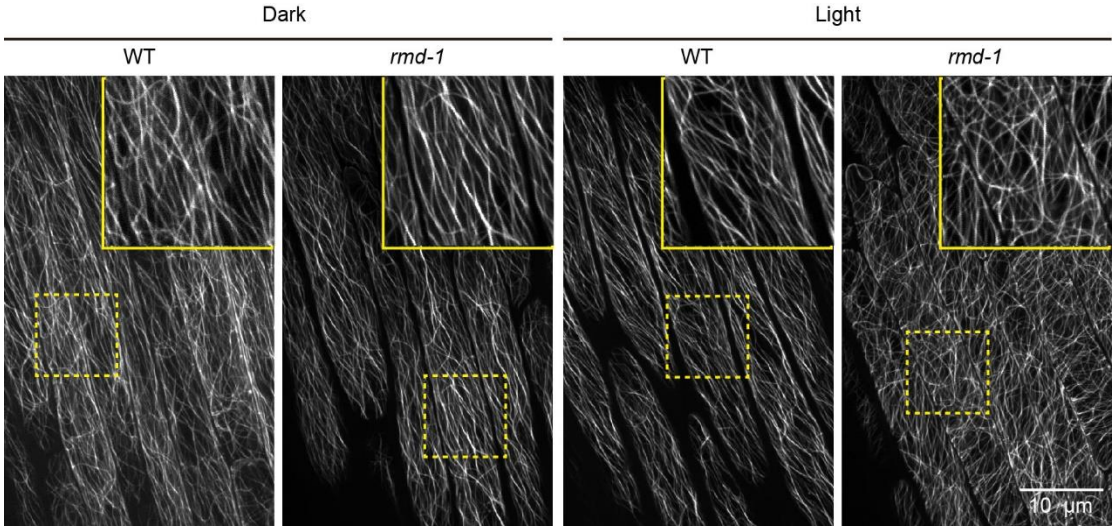

Fig. S7. The microtubule array in *rmd-1* coleoptile. The mNG-MAP4 seeds were germinated for 4 days under either dark or light condition. The images are maximum projections from epidermis. The enlargements' positons are indicated by the dashed rectangles in each large images.

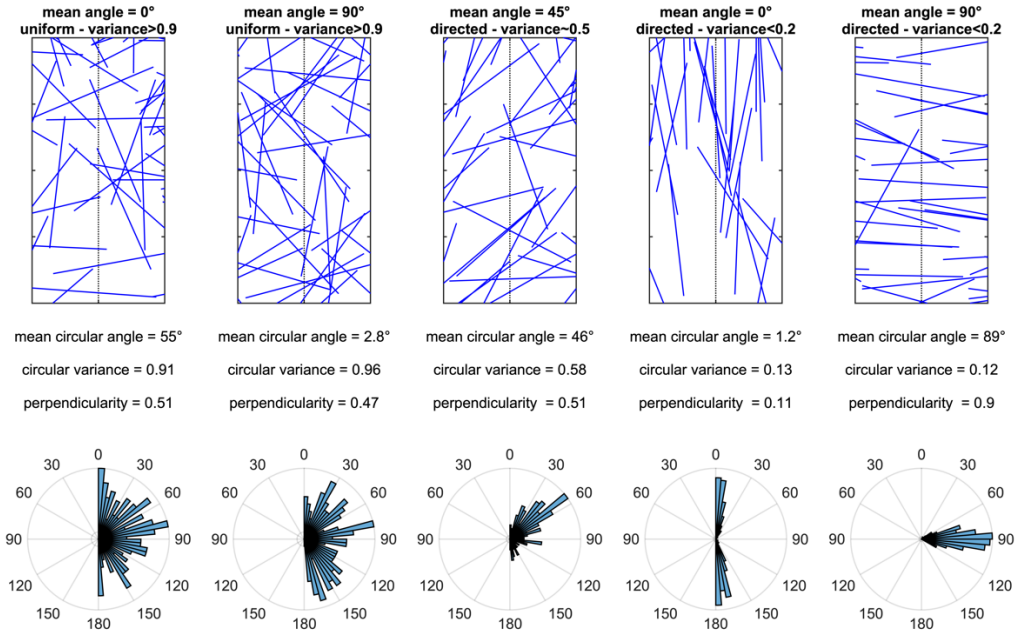

Fig. S8. Description of the circular statistics using simulated filament networks. Each column shows a simulated network (N=200; not all edges are shown) using random generated angles from a von-Mises distribution (the normal distribution in circular statistics; Berens, 2009; Fisher, 1993; Jammalamadaka and SenGupta, 2001). The values used in the simulations are: **(1)** μ=0°, κ=0; **(2)** μ=90°, κ=0; (**3**) μ=0°, κ=1; **(4)** μ=0°, κ=4; **(5)** μ=90°, κ=4. The dotted line indicates the major cell axis and all angles were restricted to 0°-180°in order to resemble edge angles that were extracted using Cytoseg2. More description is included in Materials and Methods section.

Table S1. The evaluation of rice cytoskeleton fluorescent marker constructs

Construct elements	Used elements	Evaluation
Promoter	35S	Gene silencing, usually high expression in stomata guard cells, no expression in reproductive tissues.
	ZmUbi1	Express in all tissues except pollen mother cell, no gene silencing observed.
	RUBQ2	Express in all tissues except pollen mother cell, no gene silencing observed. Expression level is higher than ZmUbi1.
Fluorescent protein	GFP	Good.
	mNeongreen	Best. Brighter than GFP.
	mScarlet	Bright but sensitive to photo-bleaching.
Actin binding protein	OsfABD	Not determined. (No signal was observed, not sure the reason)
	AtfABD	Label filamentous actin with quite dynamic.
Microtubule binding protein	OsTUA1	Weakly label microtubules in rice cells, mainly retained in cytosol, also cause plant distortion phenotype.
	MAP4	Microtubule labelling well. High expression sometimes caused plant dwarf phenotype. Normal plants can be obtained.

Table S2 The quantification of microtubule filaments in salt treated cell

Time point of salt treatment	Total filament counts	Number of analyzed cells	Mean filament per cell
1.5-2 h	1265	96	13.59
3.5-4 h	Not detectable	111	Not detectable
5.5-6 h	152	122	1.25
7.5-8 h	1903	138	13.79

Table S3. Statistical test of edge capacity using Mann–Whitney U test

Dataset	Wild type (dark)	*rmd-1* (dark)	Wild type (light)	*rmd-1* (light)
Wild type (dark)		p<0.001	p=0.005	p<0.001
rmd-1 (dark)	p<0.001		p<0.001	p<0.001
Wild type (light)	p=0.005	p<0.001		p<0.001
rmd-1 (light)	p<0.001	p<0.001	p<0.001	

* Green shading indicates significant difference with 95% confidence intervals (p<0.05)

Table S4. The used primers

Plasmid	Fragment	Primer sequence
RUBQ2/ ZmUbi::mNG-MAP4/ fABD	RUBQ2 promoter	FP ATGACCATGATTACGAATTCATTCGGGTCAAGGCGGAAGC RP GGTACCGAGCTCGAATTCCTGCAAGAAATAATCACCAA
	Zmubiquitin1 promoter	FP ATGACCATGATTACGCAGTGCAGCGTGACCCGGT RP TACCGAGCTCGAATTCGGATCCTCTAGAGTCGACCTGCAGA
	mNeongreen	FP ATTCGAGCTCGGTACCATGGTGAGCAAGGGCGA RP CGACTCTAGAGGATCCCTTGTACAGCTCGTC
	MAP4	FP GCTGTACAAGGATCCTCCCGGCAAGAAGAA RP ATTCGAGCTGGTCACCCTAGTCACCTCCTGA
	AtfABD	FP GCTGTACAAGGATCCTCTTGAAAGAGCTGAA RP ATTCGAGCTGGTCACCCTATTCGATGGATGC
RUBQ2:: mScarlet	mScarlet	FP TTCGAGCTCGGTACCATGGTGAGCAAGGGCGAGG MSCARLET-MAP4-RP TGCTTCTTCTTGCCGGGAGGATCCCTTGTACAGCTCGTC MSCARLET-FABD-RP ATTCAGCTCTTTCAAGAGGATCCCCTTGTACAGCTCGTC
ZmUbi::GFP-OsTUA1/ OsfABD	GFP	FP ATTCGAGCTCGGTACCATGGTGAGCAAGGGCGAGGA RP CTAGAGGATCCCCGGGTACCCTTGTACAGCTCGTCCATGCC
	OsTUA1	FP GCAGGCATGCAAGCTTATGAGGGAGTGCATCTCGAT RP TCACCTGTAATTCACACGTGCTAGTACTCGTCACCATCATCGC
	OsfABD	FP GCAGGCATGCAAGCTTTTCCTCAAGTCCAGTACCA RP TCACCTGTAATTCACACCTAAAGAATTAAATGAGGCCTT
35S::GFP-AtfABD/MAP4	GFP	FP CGGGGGACTCTTGACCATGGTGAGCAAGGGCGAGGA RP CCTCAGATCTACCATGCTTGTACAGCTCGTCCATGC
	AtfABD	FP AAGCATGGTAGATCTCTTGAAAGAGCTGAA RP ATTCGAGCTGGTCACCCTATTCGATGGATGCTTCCTCTGAG
	MAP4	FP AAGCATGGTAGATCTTCCCGGCAAGAAGAA RP ATTCGAGCTGGTCACCCTAGTCACCTCCTGA

Note: The homogenous sequence for infusion is underlined.

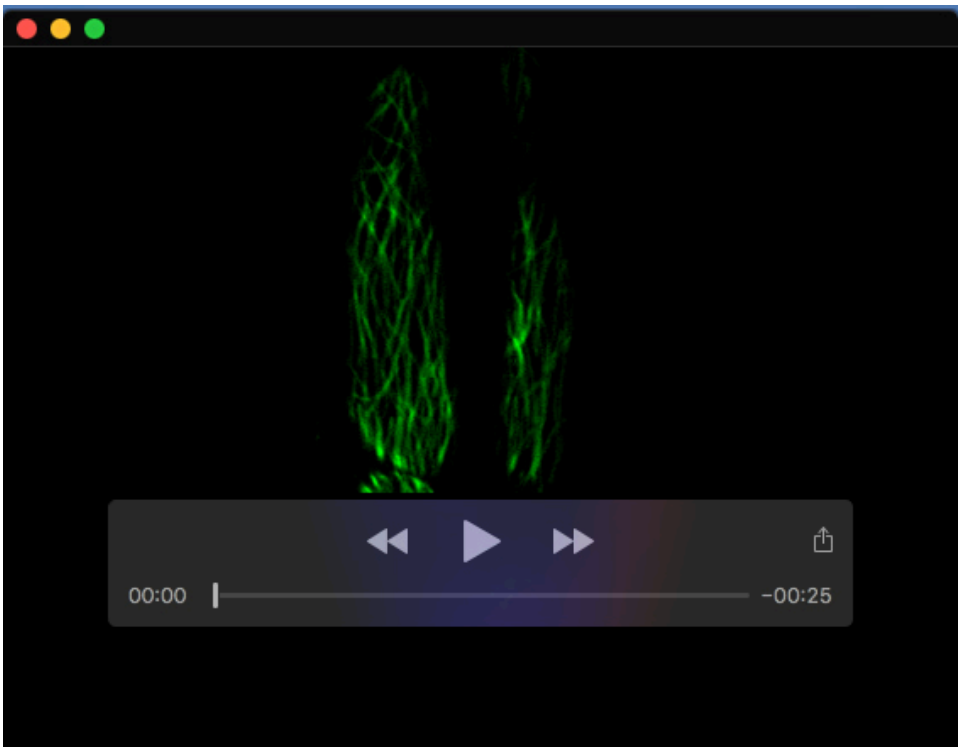

Movie 1. The time-lapse movie of mNG-MAP4 in rice coleoptile, related to Fig. 2C.

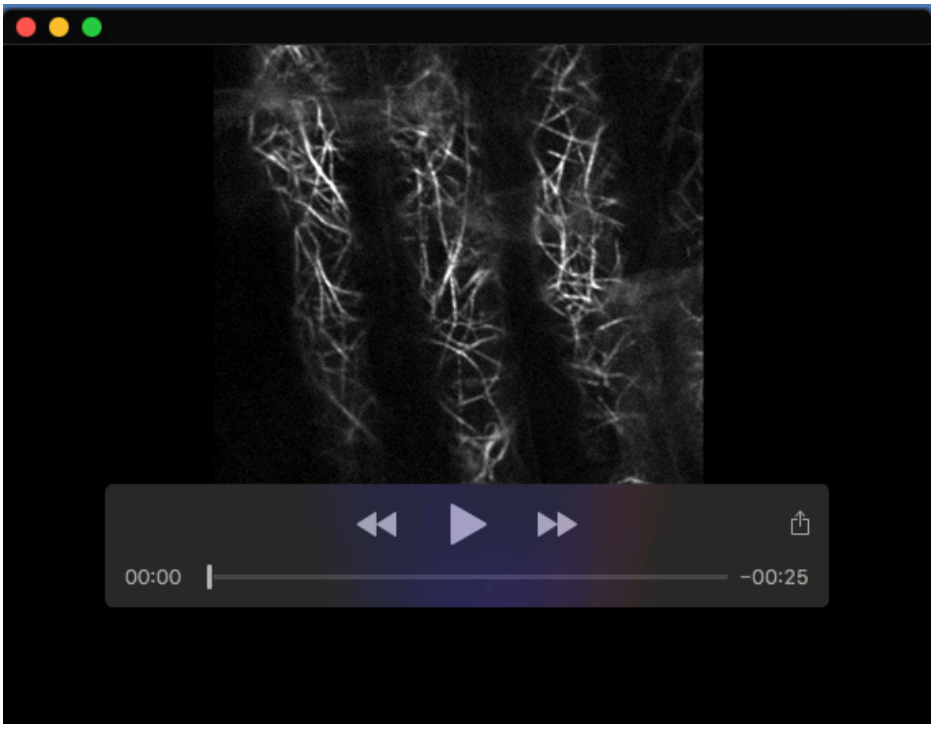

Movie 2. The time-lapse movie of mNG-fABD in rice coleoptile, related to Fig. 2E.

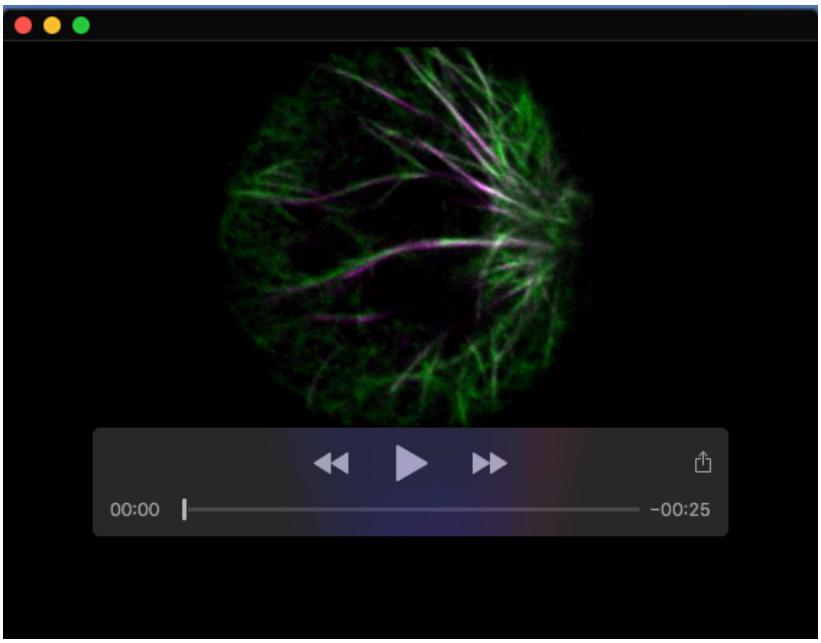

Movie 3. The time-lapse movie of mNG-fABD mScarlet-MAP4 in rice pollen, related to Fig. 4D. Please note the co-migration between two signals. mNG-fABD is in green and mScarlet-MAP4 is in magenta.

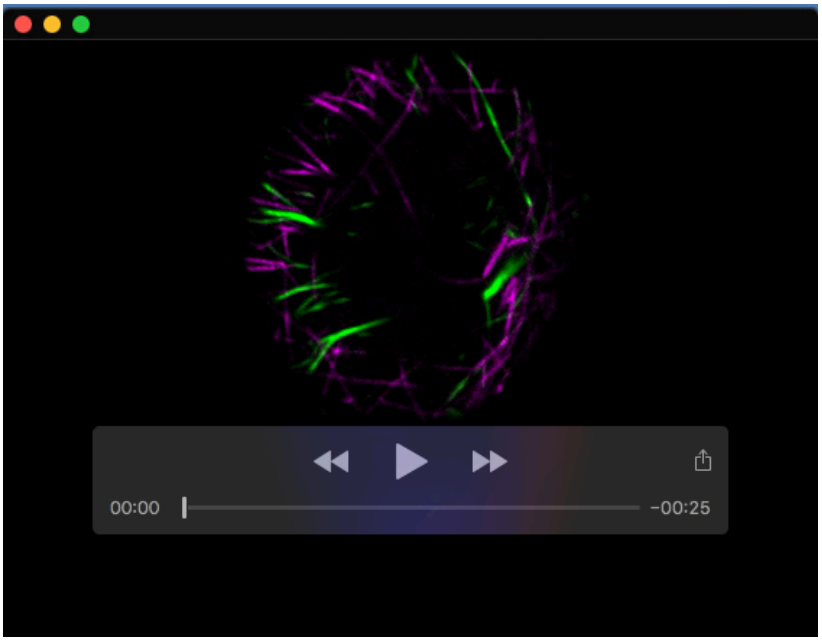

Movie 4. The time-lapse movie of mNG-fABD mScarlet-MAP4 in rice pollen treated with Latrunculin B, related to Fig. 4G. Please note the signal changes along the time.

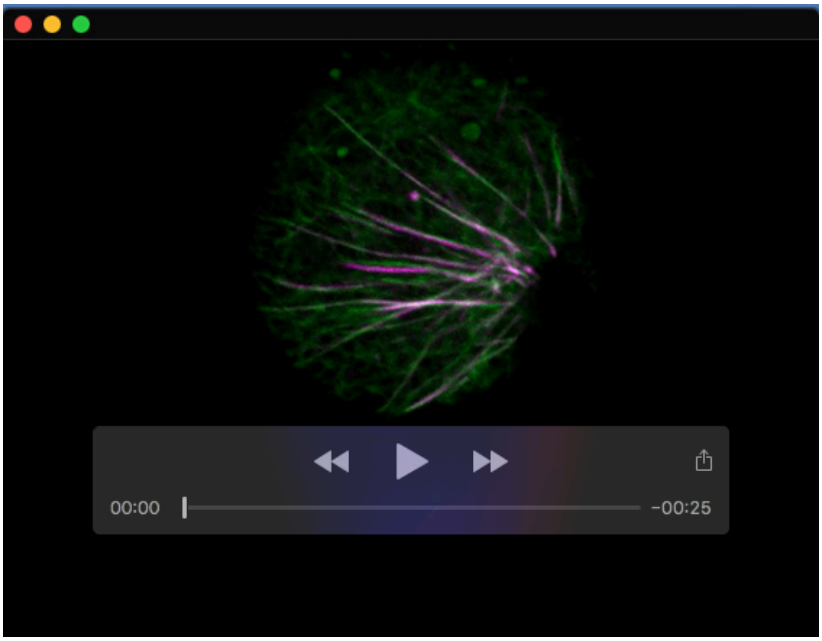

Movie 5. The time-lapse movie of mNG-fABD mScarlet-MAP4 in rice pollen treated with oryzalin, related to Fig. 4H. Please note the signal changes along the time.

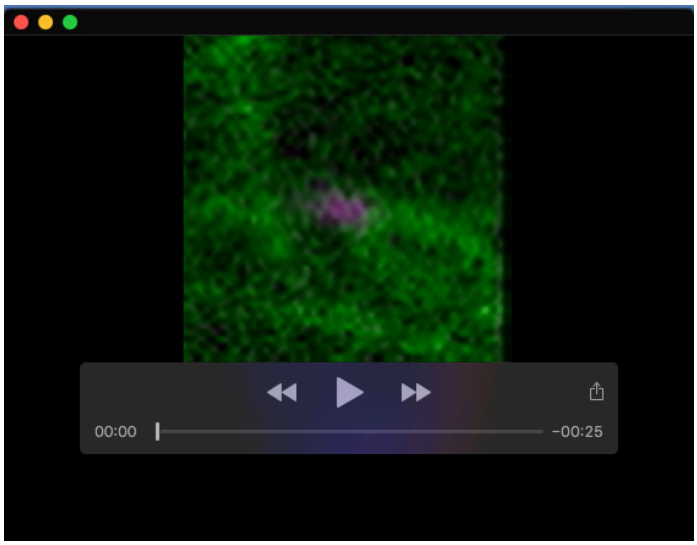

Movie 6. The time-lapse movie of mNG-fABD mScarlet-MAP4 in rice root treated with 250 mM NaCl for 1.5 h, related to Fig. 7B. Time interval is 10 sec.

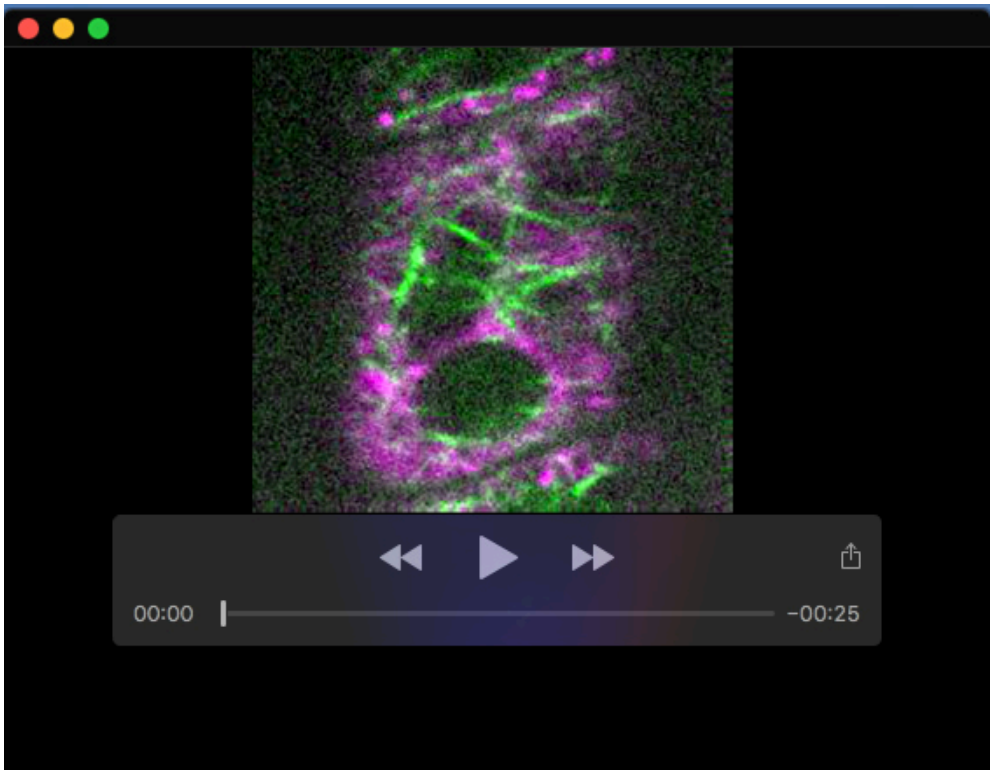

Movie 7. The time-lapse movie of mNG-fABD mScarlet-MAP4 in rice root treated with 250 mM NaCl for 5 h, related to Fig. 7D. Time interval is 10 sec.